

University of Groningen

Measurement of the branching fraction of $D_s^+ \rightarrow \ell^+ \nu_\ell$ via $e^+e^- \rightarrow D_s^{*+} D_s^{*-}$

BESIII Collaboration; Ablikim, M.; Achasov, M.N.; Adlarson, P.; Afedulidis, O.; Ai, X. C.; Aliberti, R.; Amoroso, A.; Kalantar-Nayestanaki, Nasser; Kavatsyuk, Myroslav

Published in:
Physical Review D

DOI:
[10.1103/PhysRevD.110.052002](https://doi.org/10.1103/PhysRevD.110.052002)

IMPORTANT NOTE: You are advised to consult the publisher's version (publisher's PDF) if you wish to cite from it. Please check the document version below.

Document Version
Publisher's PDF, also known as Version of record

Publication date:
2024

[Link to publication in University of Groningen/UMCG research database](#)

Citation for published version (APA):

BESIII Collaboration, Ablikim, M., Achasov, M. N., Adlarson, P., Afedulidis, O., Ai, X. C., Aliberti, R., Amoroso, A., Kalantar-Nayestanaki, N., Kavatsyuk, M., & Messchendorp, J. (2024). Measurement of the branching fraction of $D_s^+ \rightarrow \ell^+ \nu_\ell$ via $e^+e^- \rightarrow D_s^{*+} D_s^{*-}$. *Physical Review D*, 110(5), Article 052002. <https://doi.org/10.1103/PhysRevD.110.052002>

Copyright

Other than for strictly personal use, it is not permitted to download or to forward/distribute the text or part of it without the consent of the author(s) and/or copyright holder(s), unless the work is under an open content license (like Creative Commons).

The publication may also be distributed here under the terms of Article 25fa of the Dutch Copyright Act, indicated by the "Taverne" license. More information can be found on the University of Groningen website: <https://www.rug.nl/library/open-access/self-archiving-pure/taverne-amendment>.

Take-down policy

If you believe that this document breaches copyright please contact us providing details, and we will remove access to the work immediately and investigate your claim.

Downloaded from the University of Groningen/UMCG research database (Pure): <http://www.rug.nl/research/portal>. For technical reasons the number of authors shown on this cover page is limited to 10 maximum.

Measurement of the branching fraction of $D_s^+ \rightarrow \ell^+ \nu_\ell$ via $e^+ e^- \rightarrow D_s^{*+} D_s^{*-}$

M. Ablikim *et al.**
(BESIII Collaboration)

 (Received 16 July 2024; accepted 19 August 2024; published 10 September 2024)

Based on 10.64 fb^{-1} of $e^+ e^-$ collision data taken at center-of-mass energies between 4.237 and 4.699 GeV with the BESIII detector, we study the leptonic D_s^+ decays using the $e^+ e^- \rightarrow D_s^{*+} D_s^{*-}$ process. The branching fractions of $D_s^+ \rightarrow \ell^+ \nu_\ell$ ($\ell = \mu, \tau$) are measured to be $\mathcal{B}_{D_s^+ \rightarrow \mu^+ \nu_\mu} = (0.547 \pm 0.026_{\text{stat}} \pm 0.016_{\text{syst}})\%$ and $\mathcal{B}_{D_s^+ \rightarrow \tau^+ \nu_\tau} = (5.60 \pm 0.16_{\text{stat}} \pm 0.20_{\text{syst}})\%$, respectively. The product of the decay constant and Cabibbo-Kobayashi-Maskawa matrix element $|V_{cs}|$ is determined to be $f_{D_s^+} |V_{cs}| = (246.5 \pm 5.9_{\text{stat}} \pm 3.6_{\text{syst}} \pm 0.5_{\text{input}})_{\mu\nu}$ and $f_{D_s^+} |V_{cs}| = (252.7 \pm 3.6_{\text{stat}} \pm 4.5_{\text{syst}} \pm 0.6_{\text{input}})_{\tau\nu}$ MeV, respectively. Taking the value of $|V_{cs}|$ from a global fit in the Standard Model, we obtain $f_{D_s^+} = (253.2 \pm 6.0_{\text{stat}} \pm 3.7_{\text{syst}} \pm 0.6_{\text{input}})_{\mu\nu}$ and $f_{D_s^+} = (259.6 \pm 3.7_{\text{stat}} \pm 4.6_{\text{syst}} \pm 0.6_{\text{input}})_{\tau\nu}$ MeV, respectively. Conversely, taking the value for $f_{D_s^+}$ from the latest lattice quantum chromodynamics calculation, we obtain $|V_{cs}| = (0.986 \pm 0.023_{\text{stat}} \pm 0.014_{\text{syst}} \pm 0.003_{\text{input}})_{\mu\nu}$ and $|V_{cs}| = (1.011 \pm 0.014_{\text{stat}} \pm 0.018_{\text{syst}} \pm 0.003_{\text{input}})_{\tau\nu}$, respectively.

DOI: [10.1103/PhysRevD.110.052002](https://doi.org/10.1103/PhysRevD.110.052002)

I. INTRODUCTION

Experimental studies of the decays of the D_s^+ are important to understand weak and strong interactions in the charm decays. In the Standard Model (SM), the weak and strong effects in leptonic D_s^+ decays can be well separated. The partial width of the decay $D_s^+ \rightarrow \ell^+ \nu_\ell$ ($\ell = \mu, \tau$) is given by [1]

$$\Gamma_{D_s^+ \rightarrow \ell^+ \nu_\ell} = \frac{G_F^2}{8\pi} f_{D_s^+}^2 |V_{cs}|^2 m_\ell^2 m_{D_s^+} \left(1 - \frac{m_\ell^2}{m_{D_s^+}^2}\right)^2, \quad (1)$$

where G_F is the Fermi coupling constant, $f_{D_s^+}$ is the D_s^+ decay constant, $|V_{cs}|$ is the magnitude of the $c \rightarrow s$ Cabibbo-Kobayashi-Maskawa (CKM) matrix element [2], m_ℓ is the lepton mass, and $m_{D_s^+}$ is the D_s^+ meson mass. Using the measured branching fraction (BF) of $D_s^+ \rightarrow \ell^+ \nu_\ell$, the product of $f_{D_s^+} |V_{cs}|$ can be determined. By taking the latest $f_{D_s^+}$ [3] calculated by lattice quantum chromodynamics (LQCD), one can determine $|V_{cs}|$, which is an essential input for testing CKM matrix unitarity. Conversely, taking $|V_{cs}|$ from the SM global fit, one can extract $f_{D_s^+}$, which is a crucial check of LQCD calculations [3–8]. In addition, the BF ratio of $D_s^+ \rightarrow \tau^+ \nu_\tau$

and $D_s^+ \rightarrow \mu^+ \nu_\mu$ provides an important test of $\tau - \mu$ lepton-flavor universality.

In recent years, many studies of $D_s^+ \rightarrow \ell^+ \nu_\ell$ have been performed by the CLEO [9–11], BABAR [12], Belle [13], and BESIII [14–23] experiments. The BESIII Collaboration has reported experimental studies of $D_s^+ \rightarrow \ell^+ \nu_\ell$ using the $e^+ e^- \rightarrow D_s^+ D_s^-$ and $e^+ e^- \rightarrow D_s^\pm D_s^{*\mp}$ processes. These studies are based on 0.48 and 7.33 fb^{-1} of $e^+ e^-$ collision data taken at center-of-mass energies ($E_{\text{c.m.}}$) of $\sqrt{s} = 4.009$ [14] and 4.128–4.226 GeV [15–21], respectively. The latter ones are the most precise measurements to date. In this paper, we perform new measurements of the BFs of $D_s^+ \rightarrow \mu^+ \nu_\mu$ and $D_s^+ \rightarrow \tau^+ \nu_\tau$ via the $e^+ e^- \rightarrow D_s^{*+} D_s^{*-}$ process. This analysis utilizes 10.64 fb^{-1} of $e^+ e^-$ collision data collected at center-of-mass energies between $\sqrt{s} = 4.237$ and 4.699 GeV. Notably, this is the first time the $e^+ e^- \rightarrow D_s^{*+} D_s^{*-}$ process has been used to measure D_s^+ leptonic decays. Throughout this paper, charge-conjugation is always implied and ρ denotes the $\rho(770)$ meson.

II. BESIII DETECTOR AND MONTE CARLO SIMULATION

The BESIII detector is a magnetic spectrometer [24] operated at the Beijing Electron Positron Collider [25]. The cylindrical core of the BESIII detector consists of a helium-based multilayer drift chamber (MDC), a plastic scintillator time-of-flight (TOF) system, and a CsI(Tl) electromagnetic calorimeter (EMC), which are all enclosed in a superconducting solenoidal magnet providing a 1.0 T magnetic field. The solenoid is supported by an octagonal flux-return yoke with resistive plate counter muon-identifier modules

*Full author list given at the end of the article.

Published by the American Physical Society under the terms of the [Creative Commons Attribution 4.0 International license](https://creativecommons.org/licenses/by/4.0/). Further distribution of this work must maintain attribution to the author(s) and the published article's title, journal citation, and DOI. Funded by SCOAP³.

(MUC) interleaved with steel. The acceptance of charged particles and photons is 93% over the 4π solid angle. The charged-particle momentum resolution at 1 GeV/ c is 0.5%, and the resolution of specific ionization energy loss (dE/dx) is 6% for electrons from Bhabha scattering. The EMC measures photon energies with a resolution of 2.5% (5%) at 1 GeV in the barrel (end cap) region. The time resolution of the TOF barrel part is 68 ps, while that of the end cap part is 110 ps. The end cap TOF system was upgraded in 2015 using multigap resistive plate chamber technology, providing a time resolution of 60 ps [26,27]. About 74% of the data used here benefit from this upgrade. Details about the design and performance of the BESIII detector are given in Ref. [24].

Simulated samples produced with the Geant4-based [28] Monte Carlo (MC) package, which includes the geometric description of the BESIII detector and the detector response, are used to determine the detection efficiency and to estimate the backgrounds. The simulation includes the beam-energy spread and initial-state radiation in the e^+e^- annihilations modeled with the generator KKMC [29]. An inclusive MC sample with a luminosity of 20 times that of the data is produced at center-of-mass energies between 4.237 and 4.699 GeV. It includes open-charm processes, initial-state radiation production of $\psi(3770)$, $\psi(3686)$, and J/ψ , $q\bar{q}$ ($q = u, d, s$) continuum processes, along with Bhabha scattering, $\mu^+\mu^-$, $\tau^+\tau^-$, and $\gamma\gamma$ events. In the simulation, the production of open-charm processes directly via e^+e^- annihilations are modeled with the generator CONEXC [30]. The known decay modes are modeled with EvtGen [31] using the BFs taken from the Particle Data Group (PDG) [2], and the remaining unknown decays of the charmonium states are modeled by LUNDCHARM [32]. Final-state radiation is incorporated using the PHOTOS package [33]. The input energy-dependent Born cross section for $e^+e^- \rightarrow D_s^{*+}D_s^{*-}$ is based on the BESIII measurement [34].

III. ANALYSIS METHOD

In the $e^+e^- \rightarrow D_s^{*+}D_s^{*-}$ process, the D_s mesons are produced via $D_s^* \rightarrow \gamma(\pi^0)D_s$. We fully reconstruct the transition $\gamma(\pi^0)$ and the D_s^* meson in one of several hadronic decay modes; successful cases are referred to as single-tag candidates. When the single-tag D_s^{*-} and the signal D_s^{*+} decay of interest are simultaneously reconstructed, we obtain the so-called double-tag candidates. The BF of the signal decay is determined by

$$\mathcal{B}_{\text{sig}} = \frac{N_{\text{DT}}}{N_{\text{ST}} \cdot \bar{\epsilon}_{\text{sig}}}. \quad (2)$$

Here, N_{DT} is the double-tag yield in data; $N_{\text{ST}} = \sum_{i,j} N_{\text{ST}}^{i,j}$ is the total single-tag yield in data summing over the tag mode i and the energy point j ; the $\bar{\epsilon}_{\text{sig}}$ is the averaged

efficiency of the signal decay and estimated by $\bar{\epsilon}_{\text{sig}} = \sum_j [\sum_i (\frac{N_{\text{ST}}^{i,j}}{N_{\text{ST}}} \cdot \frac{\epsilon_{\text{DT}}^j}{\epsilon_{\text{ST}}^i}) \cdot \frac{N_{\text{ST}}^j}{N_{\text{ST}}}]$, where ϵ_{DT}^j and ϵ_{ST}^i are the detection efficiencies of the double- and single-tag candidates for the i th tag mode, respectively. The efficiencies include the BFs of the daughter particle decays.

IV. SINGLE-TAG D_s^{*-} CANDIDATES

The single-tag D_s^{*-} candidates are formed from the selected D_s^- candidates and a transition $\gamma(\pi^0)$. The D_s^- candidates are reconstructed from the 14 hadronic decay modes, including $D_s^- \rightarrow K^+K^-\pi^-$, $K^+K^-\pi^-\pi^0$, $\pi^+\pi^-\pi^-$, $K_S^0K^-$, $K_S^0K^-\pi^0$, $K^-\pi^+\pi^+$, $K_S^0K_S^0\pi^-$, $K_S^0K^+\pi^-\pi^-$, $K_S^0K^-\pi^+\pi^-$, $\eta_{\gamma\gamma}\pi^-$, $\eta_{\pi^0\pi^+\pi^-\pi^-}$, $\eta'_{\pi^+\pi^-\eta}\pi^-$, $\eta'_{\gamma\gamma^0}\pi^-$, and $\eta_{\gamma\gamma}\rho^-$. Here, the subscripts of the η and η' represent the decay modes used to reconstruct those states.

All charged tracks must satisfy $|\cos\theta| < 0.93$, and those not from K_S^0 decays are further required to satisfy $V_{xy} < 1$ and $|V_z| < 10$ cm, where V_{xy} and $|V_z|$ are the distance of the closest approach to the interaction point (IP) in the transverse plane and along the MDC symmetry axis, respectively, and θ is the polar angle with respect to the MDC symmetry axis. Particle identification (PID) for the charged particles combines measurements of the energy deposited in the MDC (dE/dx) and the flight time in the TOF to form likelihoods $\mathcal{L}(h)$ ($h = K, \pi$) for each hadron h hypothesis. Charged kaons and pions are identified by comparing the likelihoods for the kaon and pion hypotheses, $\mathcal{L}(K) > \mathcal{L}(\pi)$ and $\mathcal{L}(\pi) > \mathcal{L}(K)$, respectively.

Each K_S^0 candidate is reconstructed from two oppositely charged tracks satisfying $|V_z| < 20$ cm. The two charged tracks are assigned as $\pi^+\pi^-$ without imposing further PID criteria. They are constrained to originate from a common vertex and are required to have an invariant mass within $|M_{\pi^+\pi^-} - m_{K_S^0}| < 12$ MeV/ c^2 , where $m_{K_S^0}$ is the K_S^0 nominal mass [2]. The decay length of the K_S^0 candidate is required to be greater than twice the vertex resolution away from the IP.

Photon candidates are identified using isolated showers in the EMC. The deposited energy of each shower must be more than 25 MeV in the barrel region ($|\cos\theta| < 0.80$) and more than 50 MeV in the end cap region ($0.86 < |\cos\theta| < 0.92$). To exclude showers that originate from charged tracks, the angle subtended by the EMC shower and the position of the closest charged track at the EMC must be greater than 10° as measured from the IP. To suppress electronic noise and showers unrelated to the event, the difference between the EMC time and the event start time is required to be within $[0, 700]$ ns.

The π^0 and η mesons are reconstructed from photon pairs. To form π^0 and η candidates, the invariant masses of the selected photon pairs are required to be within the $M_{\gamma\gamma}$

TABLE I. The $M_{D_s^-}$ requirements, ΔE requirements, single-tag yields (N_{ST}), single-tag efficiencies (ϵ_{ST}), and various double-tag efficiencies for each tag mode at 4.260 GeV. The $\epsilon_{\text{DT}}^{\mu_a\nu}$ and $\epsilon_{\text{DT}}^{\mu_b\nu}$ correspond to the double-tag efficiencies for $D_s^+ \rightarrow \mu_a^+\nu_\mu$ and $D_s^+ \rightarrow \mu_b^+\nu_\mu$, while $\epsilon_{\text{DT}}^{\tau_e\nu}$, $\epsilon_{\text{DT}}^{\tau_\mu\nu}$, $\epsilon_{\text{DT}}^{\tau_\pi\nu}$, and $\epsilon_{\text{DT}}^{\tau_\rho\nu}$ correspond to the double-tag efficiencies for $D_s^+ \rightarrow \tau_e^+\nu_\tau$, $D_s^+ \rightarrow \tau_\mu^+\nu_\tau$, $D_s^+ \rightarrow \tau_\pi^+\nu_\tau$, and $D_s^+ \rightarrow \tau_\rho^+\nu_\tau$, respectively. The muon candidates identified with (without) MUC information are denoted by μ_a (μ_b). The efficiencies include the BFs of D_s^{*+} and τ^+ decays. The uncertainties are statistical only.

| D_s^- tag mode | $M_{D_s^-}$ (GeV/ c^2) | ΔE (MeV) | N_{ST} | ϵ_{ST} (%) | $\epsilon_{\text{DT}}^{\mu_a\nu}$ (%) | $\epsilon_{\text{DT}}^{\mu_b\nu}$ (%) | $\epsilon_{\text{DT}}^{\tau_e\nu}$ (%) | $\epsilon_{\text{DT}}^{\tau_\mu\nu}$ (%) | $\epsilon_{\text{DT}}^{\tau_\pi\nu}$ (%) | $\epsilon_{\text{DT}}^{\tau_\rho\nu}$ (%) |
|-------------------------------|---------------------------|------------------|-----------------|----------------------------|---------------------------------------|---------------------------------------|--|--|--|---|
| $K^+K^-\pi^-$ | (1.950, 1.986) | (-31, 26) | 7454 ± 125 | 19.67 ± 0.07 | 14.43 ± 0.07 | 16.89 ± 0.09 | 3.54 ± 0.02 | 1.53 ± 0.01 | 1.62 ± 0.01 | 1.07 ± 0.01 |
| $K^+K^-\pi^-\pi^0$ | (1.947, 1.982) | (-38, 29) | 2186 ± 108 | 5.15 ± 0.05 | 5.08 ± 0.06 | 5.53 ± 0.06 | 1.21 ± 0.01 | 0.55 ± 0.01 | 0.52 ± 0.01 | 0.28 ± 0.01 |
| $\pi^-\pi^+\pi^-$ | (1.952, 1.984) | (-34, 28) | 1929 ± 99 | 25.73 ± 0.26 | 18.18 ± 0.08 | 24.60 ± 0.10 | 4.32 ± 0.02 | 1.84 ± 0.01 | 2.35 ± 0.01 | 1.76 ± 0.02 |
| $K_S^0K^-$ | (1.948, 1.991) | (-33, 30) | 1649 ± 53 | 22.97 ± 0.16 | 16.44 ± 0.09 | 21.80 ± 0.11 | 3.87 ± 0.02 | 1.68 ± 0.01 | 2.07 ± 0.01 | 1.53 ± 0.02 |
| $K_S^0K^-\pi^0$ | (1.946, 1.987) | (-40, 31) | 554 ± 50 | 7.51 ± 0.14 | 6.45 ± 0.09 | 8.73 ± 0.11 | 1.54 ± 0.02 | 0.68 ± 0.01 | 0.84 ± 0.01 | 0.53 ± 0.01 |
| $K^-\pi^-\pi^+$ | (1.953, 1.983) | (-33, 28) | 1112 ± 83 | 23.47 ± 0.40 | 16.15 ± 0.17 | 21.19 ± 0.20 | 3.83 ± 0.03 | 1.66 ± 0.02 | 1.98 ± 0.02 | 1.46 ± 0.03 |
| $K_S^0K_S^0\pi^-$ | (1.951, 1.986) | (-32, 28) | 266 ± 22 | 11.07 ± 0.22 | 7.96 ± 0.14 | 10.84 ± 0.18 | 1.94 ± 0.03 | 0.83 ± 0.02 | 1.03 ± 0.02 | 0.72 ± 0.02 |
| $K_S^0K^+\pi^-\pi^-$ | (1.953, 1.983) | (-31, 26) | 808 ± 45 | 10.21 ± 0.12 | 7.46 ± 0.12 | 9.30 ± 0.14 | 1.80 ± 0.02 | 0.78 ± 0.02 | 0.88 ± 0.01 | 0.52 ± 0.02 |
| $K_S^0K^-\pi^+\pi^-$ | (1.958, 1.980) | (-31, 26) | 390 ± 40 | 9.66 ± 0.20 | 6.70 ± 0.06 | 8.51 ± 0.07 | 1.64 ± 0.01 | 0.73 ± 0.01 | 0.79 ± 0.01 | 0.50 ± 0.01 |
| $\eta_{\text{VT}}\pi^-$ | (1.930, 2.000) | (-52, 43) | 983 ± 69 | 19.33 ± 0.29 | 15.89 ± 0.08 | 22.99 ± 0.09 | 3.81 ± 0.02 | 1.63 ± 0.01 | 2.24 ± 0.01 | 1.69 ± 0.01 |
| $\eta_{\pi^+\pi^-\pi^0}\pi^-$ | (1.941, 1.990) | (-43, 34) | 269 ± 29 | 11.22 ± 0.28 | 8.47 ± 0.06 | 11.92 ± 0.07 | 2.02 ± 0.01 | 0.90 ± 0.01 | 1.14 ± 0.01 | 0.79 ± 0.01 |
| $\eta'_{\pi^+\pi^-\eta}\pi^-$ | (1.940, 1.996) | (-40, 34) | 575 ± 40 | 11.16 ± 0.18 | 8.60 ± 0.06 | 12.39 ± 0.07 | 2.05 ± 0.01 | 0.91 ± 0.01 | 1.18 ± 0.01 | 0.85 ± 0.01 |
| $\eta'_{\gamma\rho^0}\pi^-$ | (1.938, 1.992) | (-43, 33) | 1233 ± 75 | 14.00 ± 0.19 | 11.04 ± 0.07 | 15.46 ± 0.08 | 2.68 ± 0.01 | 1.17 ± 0.01 | 1.49 ± 0.01 | 1.00 ± 0.01 |
| $\eta'_{\text{VT}}\rho^-$ | (1.920, 2.006) | (-66, 49) | 2142 ± 191 | 8.07 ± 0.13 | 7.64 ± 0.06 | 11.59 ± 0.07 | 1.83 ± 0.01 | 0.80 ± 0.01 | 1.13 ± 0.01 | 0.80 ± 0.01 |

intervals (0.115, 0.150) and (0.500, 0.570) GeV/ c^2 , respectively. To improve momentum resolution and suppress background, a kinematic fit is imposed on each photon pair to constrain their invariant mass to the nominal π^0 or η mass [2]. The χ^2 of this kinematic fit is required to be less than 20.

The η candidates are also formed from $\pi^0\pi^+\pi^-$ combinations with invariant masses in the interval (0.530, 0.570) GeV/ c^2 . The η' candidates are formed from the $\eta\pi^+\pi^-$ and $\gamma\rho^0$ combinations with invariant masses in the intervals (0.946, 0.970) and (0.940, 0.976) GeV/ c^2 , respectively. In addition, the minimum energy of the γ from $\eta' \rightarrow \gamma\rho^0$ decays must be greater than 0.1 GeV. The ρ^0 and ρ^+ candidates are reconstructed from the $\pi^+\pi^-$ and $\pi^+\pi^0$ combinations with invariant masses within the common interval (0.570, 0.970) GeV/ c^2 .

To reject the peaking background events from $D_s^- \rightarrow K_S^0(\rightarrow \pi^+\pi^-)\pi^-$ and $D_s^- \rightarrow K_S^0(\rightarrow \pi^+\pi^-)K^-$ in the tag modes of $D_s^- \rightarrow \pi^+\pi^-\pi^-$ and $D_s^- \rightarrow K^+\pi^+\pi^-$, we require that the invariant mass of any $\pi^+\pi^-$ combination satisfy $|M_{\pi^+\pi^-} - m_{K_S^0}| > 0.03$ GeV/ c^2 .

The tagged D_s^- candidates are required to fall in the $M_{D_s^-}$ mass windows shown in the second column of Table I, following Refs. [35,36]. To further distinguish the single-tag D_s^{*-} from combinatorial background, we use two kinematic variables: the energy difference defined as

$$\Delta E = E_{\text{tag}} - E_{\text{beam}} \quad (3)$$

and the beam-constrained mass defined as

$$M_{\text{BC}} = \sqrt{E_{\text{beam}}^2/c^4 - |\vec{p}_{\text{tag}}|^2/c^2}, \quad (4)$$

where E_{beam} is the beam energy, and E_{tag} and \vec{p}_{tag} are the energy and momentum of the single-tag D_s^{*-} candidate in the rest frame of the initial e^+e^- beams.

The ΔE values for each tag mode must be within the ranges listed in Table I. If multiple γ/π^0 or D_s combinations remain, we keep only the candidates with the minimum $|\Delta E|$ for each tag mode and each D_s^* charge from a given event. For each tag mode, the single-tag yield is obtained by a fit to the corresponding M_{BC} spectrum. The signal is described by the simulated shape convolved with a Gaussian function representing the difference in resolution between data and simulation. Because the end point above 4.450 GeV is far away from the nominal D_s^* mass, the data at all energy points above 4.450 GeV are combined into one dataset. For the datasets taken below and above 4.450 GeV, the nonpeaking background shapes are modeled by an ARGUS function [37] and a second-order Chebyshev polynomial function, respectively, which have been validated by analyzing the inclusive MC sample. As an example, the M_{BC} distributions of accepted single-tag candidates for various tag modes and the fit results at 4.260 GeV are shown in Fig. 1. The candidates in the signal regions, denoted as the red arrows in each subfigure, are kept for further analysis. The resulting single-tag yields (N_{ST}^i) for various tag modes and the corresponding single-tag efficiencies (ϵ_{ST}^i) at 4.260 GeV are shown in Table I. Information for data from other energies is given in the Appendix. The total single-tag yields at the different energy points are summarized in Table II.

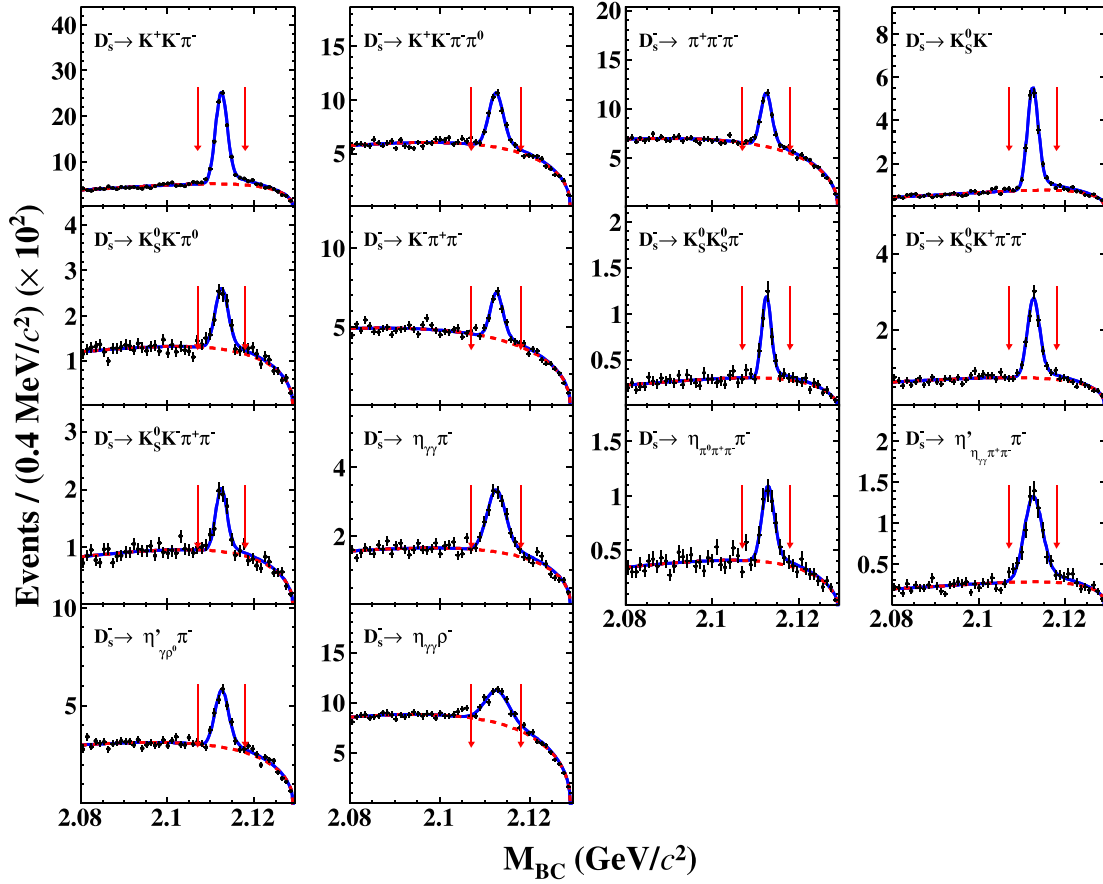


FIG. 1. Fits to the M_{BC} distributions of the single-tag D_s^{*-} candidates, where the points with error bars are data at 4.260 GeV, the blue solid curves show the best fits, and the red dashed curves show the fitted combinatorial background shapes. The pairs of arrows denote the M_{BC} signal window.

TABLE II. The integrated luminosities \mathcal{L} , the M_{BC} requirements, and the single-tag yields in data N_{ST} , for various energy points. The uncertainties are statistical only.

| $E_{c.m.}$ (GeV) | \mathcal{L} (pb $^{-1}$) | M_{BC} (GeV/ c^2) | N_{ST} |
|------------------|-----------------------------|------------------------|-------------------|
| 4.237 | 530.3 | (2.107, 2.117) | 6477 ± 163 |
| 4.246 | 593.9 | (2.107, 2.118) | 11944 ± 246 |
| 4.260 | 828.4 | (2.107, 2.118) | 21550 ± 320 |
| 4.270 | 531.1 | (2.107, 2.118) | 13319 ± 244 |
| 4.280 | 175.7 | (2.106, 2.119) | 4063 ± 152 |
| 4.290 | 502.4 | (2.106, 2.119) | 9316 ± 221 |
| 4.310–4.315 | 546.3 | (2.106, 2.119) | 5758 ± 228 |
| 4.400 | 507.8 | (2.106, 2.119) | 1855 ± 87 |
| 4.420 | 1090.7 | (2.106, 2.121) | 14890 ± 443 |
| 4.440 | 569.9 | (2.106, 2.121) | 9699 ± 443 |
| 4.470–4.699 | 4768.3 | (2.104, 2.123) | 25156 ± 762 |
| Sum | | | 124027 ± 1121 |

V. ANALYSIS OF LEPTONIC D_s^+ DECAYS

A. Selection of double-tag events

The candidates for D_s^{*+} containing a leptonic D_s^+ decay are reconstructed from the unused showers and tracks remaining after the single-tag selection. We require that only one additional track remains after the tag reconstruction. To further suppress hadronic background, we require that there is no extra charged track in each candidate event: $N_{\text{extra}}^{\text{charge}} = 0$. The transition $\gamma(\pi^0)$ is selected with the same selection criteria as the tag side.

Throughout this paper, the μ_a^+ denotes the μ^+ candidates identified with MUC information, the μ_b^+ denotes the μ^+ candidates identified without MUC information; and the τ_e^+ , τ_μ^+ , τ_π^+ , and τ_ρ^+ denote the τ^+ candidates reconstructed via $\tau^+ \rightarrow e^+ \nu_e \bar{\nu}_\tau$, $\tau^+ \rightarrow \mu^+ \nu_\mu \bar{\nu}_\tau$, $\tau^+ \rightarrow \pi^+ \bar{\nu}_\tau$, and $\tau^+ \rightarrow \rho^+ \bar{\nu}_\tau$, respectively. In the selection of the candidates for

TABLE III. The $\cos\theta_{\mu^+}$ and p_{μ^+} dependent requirements on d_{μ^+} for muon candidates.

| $ \cos\theta_{\mu^+} $ | p_{μ^+} (GeV/c) | d_{μ^+} (cm) |
|------------------------|---------------------------|-------------------------------------|
| (0.00, 0.20) | $p_{\mu^+} \leq 0.88$ | $d_{\mu^+} > 17.0$ |
| | $0.88 < p_{\mu^+} < 1.04$ | $d_{\mu^+} > 100.0p_{\mu^+} - 71.0$ |
| | $p_{\mu^+} \geq 1.04$ | $d_{\mu^+} > 33.0$ |
| (0.20, 0.40) | $p_{\mu^+} \leq 0.91$ | $d_{\mu^+} > 17.0$ |
| | $0.91 < p_{\mu^+} < 1.07$ | $d_{\mu^+} > 100.0p_{\mu^+} - 74.0$ |
| | $p_{\mu^+} \geq 1.07$ | $d_{\mu^+} > 33.0$ |
| (0.40, 0.60) | $p_{\mu^+} \leq 0.94$ | $d_{\mu^+} > 17.0$ |
| | $0.94 < p_{\mu^+} < 1.10$ | $d_{\mu^+} > 100.0p_{\mu^+} - 77.0$ |
| | $p_{\mu^+} \geq 1.10$ | $d_{\mu^+} > 33.0$ |
| (0.60, 0.80) | ... | $d_{\mu^+} > 17.0$ |
| (0.80, 0.93) | ... | $d_{\mu^+} > 17.0$ |

$D_s^+ \rightarrow \tau_\pi^+ \nu_\tau$ and $D_s^+ \rightarrow \tau_\rho^+ \nu_\tau$, the π^+ and ρ^+ candidates are selected with the same selection criteria as those used on the tag side. To select the candidates for $D_s^+ \rightarrow \tau_e^+ \nu_\tau$, the positron PID uses the measured information in the MDC, TOF, and EMC. The combined likelihoods (\mathcal{L}') under the positron, pion, and kaon hypotheses are obtained. Positron candidates are required to satisfy $\mathcal{L}'(e) > 0.001$ and $\mathcal{L}'(e)/(\mathcal{L}'(e) + \mathcal{L}'(\pi) + \mathcal{L}'(K)) > 0.8$. To select the candidates for $D_s^+ \rightarrow \tau_\mu^+ \nu_\tau$, the muon candidate is required to have a deposited energy in the EMC within (0.1, 0.3) GeV. It must also satisfy a requirement on the hit depth, d_{μ^+} , in the muon counter which depends on both $|\cos\theta_{\mu^+}|$ and p_{μ^+} . These requirements on d_{μ^+} are shown in Table III. The selected $D_s^+ \rightarrow \tau_\pi^+ \nu_\tau$ candidates offer an opportunity to determine the BF of $D_s^+ \rightarrow \mu_b^+ \nu_\mu$ as a cross check.

Information concerning the undetectable neutrino(s) is inferred by the kinematic quantity $M_{\text{miss}}^2 \equiv E_{\text{miss}}^2/c^4 - |\vec{p}_{\text{miss}}|^2/c^2$, where E_{miss} and \vec{p}_{miss} are the missing energy and momentum of the neutrino(s) candidate, respectively, calculated by $E_{\text{miss}} \equiv E_{\text{beam}} - E_k$ and $\vec{p}_{\text{miss}} \equiv -\vec{p}_{D_s^{*-}} - \vec{p}_{\gamma(\pi^0)} - \vec{p}_k$ in the e^+e^- center-of-mass frame. The index k denotes the e^+ , μ^+ , π^+ , or ρ^+ of the signal candidate, and E_k and \vec{p}_k are its energy and momentum, respectively. For $D_s^+ \rightarrow \mu_a^+ \nu_\mu$, to improve the M_{miss}^2 resolution, we perform a kinematic fit that constrains the masses of all possible particles and the missing neutrino combinations to the known mass of D_s^{*-} or D_s^{*+} . If there is more than one combination, the one with the minimum χ^2 values of the kinematic fit is retained for further analysis. The variable $E_{\text{sum}}^{\text{extra}\gamma}$ is defined as the total energy of good showers in the EMC including the transition $\gamma(\pi^0)$ used to reconstruct the signal D_s^{*+} , but excluding those used in the tag side. We also remove bremsstrahlung photon candidates, defined as showers reconstructed within 10° of the initial positron track direction.

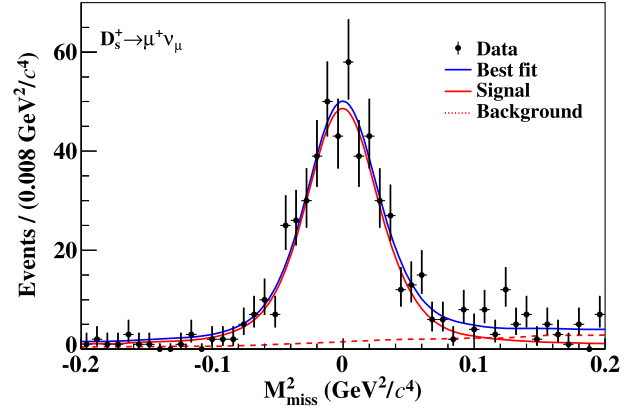


FIG. 2. Fit to the M_{miss}^2 distribution of the candidate events for $D_s^+ \rightarrow \mu^+ \nu_\mu$ with the μ^+ depth requirement. The points with error bars represent data combined from all energy points. The blue solid curve denotes the total fit. The red solid curves and red dashed curves show the fitted signal and combinatorial background shapes.

Figure 2 shows the M_{miss}^2 distribution of the candidate events for $D_s^+ \rightarrow \mu_a^+ \nu_\mu$. The left two plots of Fig. 3 show the $E_{\text{sum}}^{\text{extra}\gamma}$ distributions of the candidate events for $D_s^+ \rightarrow \tau_e^+ \nu_\tau$ and $D_s^+ \rightarrow \tau_\mu^+ \nu_\tau$, and the right two plots of Fig. 3 show the M_{miss}^2 distributions of the candidate events for $D_s^+ \rightarrow \tau_\pi^+ \nu_\tau$ and $D_s^+ \rightarrow \tau_\rho^+ \nu_\tau$. Different signal variables are chosen for the different τ^+ modes mainly to achieve better separation between signal and background. There are no prominent peaking backgrounds for $D_s^+ \rightarrow \tau_e^+ \nu_\tau$ and $D_s^+ \rightarrow \tau_\mu^+ \nu_\tau$, while the main peaking backgrounds are from $D_s^+ \rightarrow \mu^+ \nu_\mu$ and $D_s^+ \rightarrow K^0 \pi^+$ for $D_s^+ \rightarrow \tau_\pi^+ \nu_\tau$, and the main peaking backgrounds are from $D_s^+ \rightarrow \eta \pi^+ \pi^0$ and $D_s^+ \rightarrow K^0 \pi^+ \pi^0$ for $D_s^+ \rightarrow \tau_\rho^+ \nu_\tau$. These distributions are obtained from the combined data from all energy points.

B. Detection efficiencies

The detection efficiencies $\epsilon_{\text{ST}}^{ij}$ and $\epsilon_{\text{DT}}^{ij}$ are estimated by analyzing MC samples with the relevant combinations of events and appropriate relative BFs. The single-tag MC sample is generated with inclusive D_s^{*-} decays and D_s^- decays to the tag modes, while the double-tag has D_s^{*-} decays to signal modes and D_s^- decays to the tag modes, and $D_s^{*+} \rightarrow$ anything with D_s^+ decays to signal modes. As an example, the double-tag efficiencies obtained for each signal decay at 4.260 GeV are shown in Table I. For a given tag mode i and energy point j , the effective signal efficiencies $\bar{\epsilon}_{\text{sig}}^{ij}$ of each signal decay are obtained by dividing the $\epsilon_{\text{DT}}^{ij}$ by $\epsilon_{\text{ST}}^{ij}$. For each signal decay, the averaged signal efficiencies $\bar{\epsilon}_{\text{sig}}$ are obtained by weighting them by the relative single-tag yields N_{ST}^{ij} ; the results are shown in Table IV.

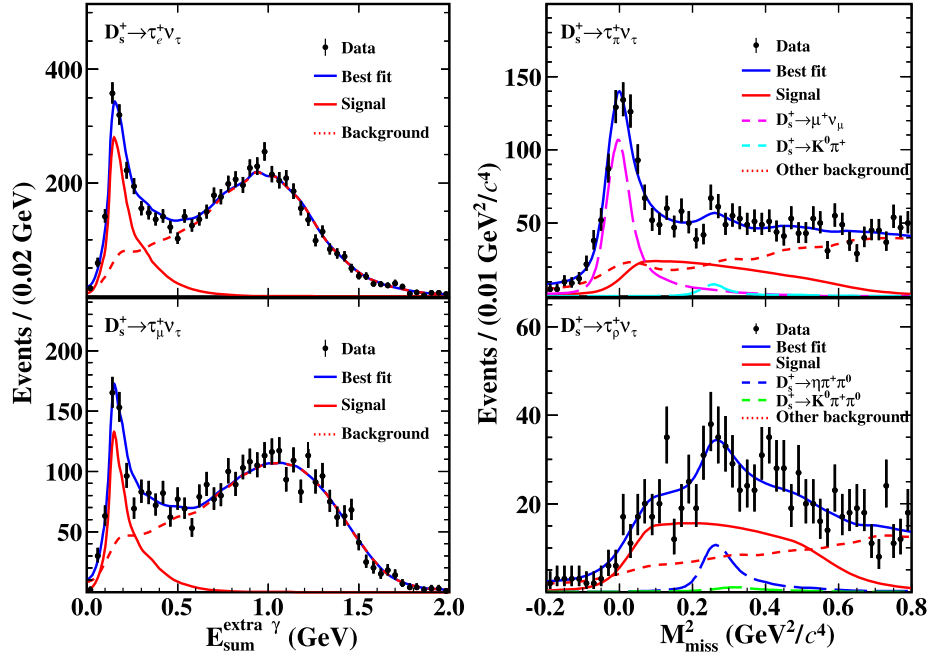


FIG. 3. Simultaneous fit to the $E_{\text{sum}}^{\text{extra}\gamma}$ distributions (left) of $D_s^+ \rightarrow \tau_e^+ \nu_\tau$ and $D_s^+ \rightarrow \tau_\mu^+ \nu_\tau$ as well as the M_{miss}^2 distributions (right) of $D_s^+ \rightarrow \tau_\pi^+ \nu_\tau$ and $D_s^+ \rightarrow \tau_\rho^+ \nu_\tau$. The points with error bars represent data combined from all energy points. The blue solid curves denote the total fit. The red solid curves and red dashed curves show the fitted combinatorial background shapes. The pink dashed, cyan dashed, blue dashed, and green dashed are the backgrounds from $D_s^+ \rightarrow \mu^+ \nu_\mu$, $D_s^+ \rightarrow K^0 \pi^+$, $D_s^+ \rightarrow \eta \pi^+ \pi^0$, and $D_s^+ \rightarrow K^0 \pi^+ \pi^0$, respectively.

C. Branching fractions without lepton universality constraint

When using the MUC information to identify muon candidates, the background level of $D_s^+ \rightarrow \mu_a^+ \nu_\mu$ is very low. In this case, the signal yield of $D_s^+ \rightarrow \mu_a^+ \nu_\mu$ is obtained from the unbinned maximum likelihood fit to the M_{miss}^2 distribution, as shown in Fig. 2. In this fit, the signal and background shapes are modeled by the simulated shapes. We obtain a signal yield of 507 ± 26 . Combining this yield, the detection efficiency, and the single-tag yield, we use Eq. (2) to obtain the BF of $D_s^+ \rightarrow \mu_a^+ \nu_\mu$ result,

$$\mathcal{B}_{D_s^+ \rightarrow \mu_a^+ \nu_\mu} = (0.547 \pm 0.026_{\text{stat}} \pm 0.016_{\text{syst}})\%.$$

The systematic uncertainties in the BF measurement are discussed in the following section.

To extract the BF of $D_s^+ \rightarrow \tau^+ \nu_\tau$, we perform a simultaneous fit to the $E_{\text{sum}}^{\text{extra}\gamma}$ distributions of candidates for $D_s^+ \rightarrow \tau_\ell^+ \nu_\tau$ ($\ell = e$ or μ) and the M_{miss}^2 distributions of candidates for $D_s^+ \rightarrow \tau_h^+ \nu_\tau$, ($h = \pi^+$ or ρ^+), as shown in Fig. 3. There is large component of $D_s^+ \rightarrow \mu_b^+ \nu_\mu$ in the accepted candidates $D_s^+ \rightarrow \tau_\pi^+ \nu_\tau$ due to the poorer separation of muons and pions when using only the dE/dx , TOF, and EMC

TABLE IV. The signal yields, the effective signal efficiencies ($\bar{\epsilon}_{\text{sig}}$), and the obtained BFs. The efficiencies include the BFs of all subresonant decays. The first uncertainties are statistical and the second systematic. The high effective signal efficiency for $D_s^+ \rightarrow \mu^+ \nu_\mu$ is mainly due to the fact that the tag environments in the signal MC sample are very different from the inclusive MC sample, where the single-tag efficiency is affected much more due to low momentum photon(s) and pions.

| Signal decay | $\bar{\epsilon}_{\text{sig}}$ (%) | No lepton universality constraint | | Lepton universality constraint | |
|--|-----------------------------------|-----------------------------------|-----------------------------|--------------------------------|-------------------------------|
| | | N_{DT} | \mathcal{B} (%) | $N_{\text{DT}}^{\text{SM}}$ | \mathcal{B}^{SM} (%) |
| $D_s^+ \rightarrow \tau_e^+ \nu_\tau$ | 7.81 ± 0.02 | | | | |
| $D_s^+ \rightarrow \tau_\mu^+ \nu_\tau$ | 18.57 ± 0.04 | | | | |
| $D_s^+ \rightarrow \tau_\pi^+ \nu_\tau$ | 8.93 ± 0.02 | 2845 ± 83 | $5.60 \pm 0.16 \pm 0.20$ | 2754 ± 69 | $5.39 \pm 0.14 \pm 0.20$ |
| $D_s^+ \rightarrow \tau_\rho^+ \nu_\tau$ | 6.11 ± 0.02 | | | | |
| $D_s^+ \rightarrow \mu_b^+ \nu_\mu$ | 94.76 ± 0.20 | 579 ± 34 | $0.491 \pm 0.029 \pm 0.020$ | 641 ± 16 | $0.553 \pm 0.014 \pm 0.021$ |
| $D_s^+ \rightarrow \mu_a^+ \nu_\mu$ | 74.67 ± 0.16 | 507 ± 26 | $0.547 \pm 0.026 \pm 0.016$ | ... | ... |

information. The signal shapes of $D_s^+ \rightarrow \mu_a^+ \nu_\mu$, $D_s^+ \rightarrow \mu_b^+ \nu_\mu$, $D_s^+ \rightarrow \tau_e^+ \nu_\tau$, and $D_s^+ \rightarrow \tau_\mu^+ \nu_\tau$ are modeled by the individual simulated shapes for each decay mode. The signal shapes of $D_s^+ \rightarrow \tau_\pi^+ \nu_\tau$ and $D_s^+ \rightarrow \tau_\rho^+ \nu_\tau$ are described by a sum of two bifurcated-Gaussian functions, whose parameters are determined from the fits to the signal MC events and are fixed in the simultaneous fit. The background components for each signal decay are modeled with shapes derived from the relevant MC simulation. The four τ^+ decay modes are constrained to have a common BF for $D_s^+ \rightarrow \tau^+ \nu_\tau$, taking into account different efficiencies and daughter particle decay BFs. From this simultaneous fit, we obtain

$$\mathcal{B}_{D_s^+ \rightarrow \mu_b^+ \nu_\mu} = (0.493 \pm 0.029_{\text{stat}} \pm 0.020_{\text{syst}})\%$$

and

$$\mathcal{B}_{D_s^+ \rightarrow \tau^+ \nu_\tau} = (5.60 \pm 0.16_{\text{stat}} \pm 0.20_{\text{syst}})\%,$$

which correspond to total signal yields of 579 ± 34 and 2845 ± 83 , respectively. The systematic uncertainties in the BF measurements are discussed in the following section.

D. Branching fractions with lepton universality constraint

The ratio of decay widths between $D_s^+ \rightarrow \tau^+ \nu_\tau$ and $D_s^+ \rightarrow \mu^+ \nu_\mu$ is given by

$$R = \frac{\Gamma_{D_s^+ \rightarrow \tau^+ \nu_\tau}}{\Gamma_{D_s^+ \rightarrow \mu^+ \nu_\mu}} = \frac{m_\tau^2 \left(1 - \frac{m_\tau^2}{m_{D_s}^2}\right)^2}{m_\mu^2 \left(1 - \frac{m_\mu^2}{m_{D_s}^2}\right)^2}. \quad (5)$$

In this ratio, $f_{D_s^+}$ and $|V_{cs}|$ cancel, and we can obtain a very precise SM prediction of $R = 9.75 \pm 0.01$, with the μ^+ and τ^+ masses from the PDG [2]. To improve the precision of the measured $f_{D_s^+}|V_{cs}|$, we have examined the BFs of $D_s^+ \rightarrow \mu^+ \nu_\mu$ and $D_s^+ \rightarrow \tau^+ \nu_\tau$ after further constraining the ratio $\mathcal{B}_{D_s^+ \rightarrow \tau^+ \nu_\tau} / \mathcal{B}_{D_s^+ \rightarrow \mu^+ \nu_\mu}$ to be 9.75 based on the SM prediction, in the fits to individual distributions in Fig. 3. From this constrained fit, the BFs of $D_s^+ \rightarrow \mu^+ \nu_\mu$ and $D_s^+ \rightarrow \tau^+ \nu_\tau$ are obtained to be

$$\mathcal{B}_{D_s^+ \rightarrow \mu^+ \nu_\mu}^{\text{SM}} = (0.553 \pm 0.014_{\text{stat}} \pm 0.021_{\text{syst}})\%$$

and

$$\mathcal{B}_{D_s^+ \rightarrow \tau^+ \nu_\tau}^{\text{SM}} = (5.39 \pm 0.14_{\text{stat}} \pm 0.20_{\text{syst}})\%,$$

respectively. These correspond to signal yields of $D_s^+ \rightarrow \mu^+ \nu_\mu$ and $D_s^+ \rightarrow \tau^+ \nu_\tau$ to be 641 ± 16 and 2754 ± 69 . The systematic uncertainties in the BF measurements are discussed in the following section.

VI. SYSTEMATIC UNCERTAINTIES

The systematic uncertainties associated with the single-tag selection cancel. Several other sources of systematic uncertainties are estimated for the BFs measurements and described below.

A. Individual systematic sources

1. Single-tag yield

To estimate the systematic uncertainty in the fitted single-tag yield, we perform fits to the M_{BC} distributions of the data and inclusive MC sample with alternative signal and background shapes. The nominal signal shape is the simulated shape convolved with a Gaussian function. An alternative signal shape is obtained after requiring that the angle between each reconstructed and generated track is less than 20° . The background shape is changed to a third-order Chebyshev polynomial. The relative differences of the ST yields between data and the inclusive MC sample from these two variations are added in quadrature assigned as the systematic uncertainty. In addition, the uncertainty due to the background fluctuation of the fitted single-tag yield is considered as an additional systematic uncertainty. The quadrature sum of these two items, 1.88%, is assigned as the systematic uncertainty in the single-tag yield.

2. Tracking and PID of e^+ , μ^+ , and π^+

The efficiencies for tracking and PID of the e^+ and μ^+ are studied with the control samples of $e^+ e^- \rightarrow \gamma e^+ e^-$ and $e^+ e^- \rightarrow \gamma \mu^+ \mu^-$, respectively. To consider the difference of topologies between $e^+ e^- \rightarrow \gamma \ell^+ \ell^-$ and $D_s^+ \rightarrow \ell^+ \nu_\ell$, the obtained efficiencies in different polar angles and momentum intervals of the control samples are reweighted to match the $D_s^+ \rightarrow \ell^+ \nu_\ell$ signals. The data-MC differences of the weighted efficiencies of e^+ tracking, and e^+ PID, μ^+ tracking, and μ^+ PID are summarized in Table V.

TABLE V. Data-MC differences of the weighted efficiencies of tracking and PID for e^+ and μ^+ .

| Signal decay | e^+ tracking | e^+ PID | μ^+ tracking | μ^+ PID |
|---|------------------|------------------|------------------|------------------|
| $D_s^+ \rightarrow \mu_a^+ \nu_\mu$ | ... | ... | 99.93 ± 0.12 | 88.62 ± 0.63 |
| $D_s^+ \rightarrow \mu_b^+ \nu_\mu$ | ... | ... | 99.93 ± 0.12 | 99.52 ± 0.53 |
| $D_s^+ \rightarrow \tau_e^+ \nu_\tau$ | 99.84 ± 0.08 | 98.45 ± 0.54 | ... | ... |
| $D_s^+ \rightarrow \tau_\mu^+ \nu_\tau$ | ... | ... | 99.93 ± 0.12 | 89.05 ± 1.06 |

TABLE VI. Relative systematic uncertainties (%) in the measurements of the BFs of $D_s^+ \rightarrow \mu^+ \nu_\mu$ and $D_s^+ \rightarrow \tau^+ \nu_\tau$.

| Source | $D_s^+ \rightarrow \mu_a^+ \nu_\mu$ | $D_s^+ \rightarrow \mu_b^+ \nu_\mu$ | $D_s^+ \rightarrow \tau^+ \nu_\tau$ | $D_s^+ \rightarrow \ell^+ \nu_\ell$ (SM) |
|---|-------------------------------------|-------------------------------------|-------------------------------------|--|
| Single-tag yield | 1.88 | 1.88 | 1.88 | 1.88 |
| μ^+ tracking | 0.19 | 0.19 | 0.04 | 0.08 |
| μ^+ PID | 0.63 | 1.06 | 0.21 | 0.99 |
| e^+ tracking | ... | ... | 0.11 | 0.10 |
| e^+ PID | ... | ... | 0.24 | 0.18 |
| π^+ tracking | ... | ... | 0.35 | 0.18 |
| π^+ PID | ... | ... | 0.08 | 0.04 |
| γ/π^0 reconstruction | 1.00 | 1.00 | 1.00 | 1.00 |
| π^0 reconstruction from ρ^+ | ... | ... | 0.29 | 0.19 |
| $E_{\text{sum}}^{\text{extra}\gamma}$ and $N_{\text{extra}}^{\text{charge}}$ requirements | ... | 0.40 | 0.56 | 0.37 |
| M_{miss}^2 fit and $E_{\text{sum}}^{\text{extra}\gamma}$ fit | 1.20 | 3.03 | 2.45 | 2.67 |
| Tag bias | 1.28 | 1.19 | 1.16 | 0.83 |
| MC statistics | 0.40 | 0.40 | 0.25 | 0.22 |
| Quoted BFs | 0.30 | 0.46 | 0.33 | 0.33 |
| SM constraint | ... | ... | ... | 0.04 |
| Total | 2.88 | 4.13 | 3.59 | 3.74 |

After correcting for the data-MC differences, the residual uncertainties are taken as individual systematic uncertainties, as listed in Table VI.

The efficiencies of the π^+ tracking and PID are studied with control samples of $e^+e^- \rightarrow K^+K^-\pi^+\pi^-(\pi^0)$ and $\pi^+\pi^-\pi^+\pi^-(\pi^0)$. The systematic uncertainties of the π^+ tracking and PID efficiencies are assigned to be 0.35% and 0.08%, respectively.

3. $\gamma(\pi^0)$ selection

The photon selection efficiency was previously studied with $J/\psi \rightarrow \pi^+\pi^-\pi^0$ decays [38]. The π^0 reconstruction efficiency was previously studied with $e^+e^- \rightarrow K^+K^-\pi^+\pi^-\pi^0$ events. The systematic uncertainty of finding the transition γ or π^0 , weighted according to the BFs for $D_s^{*+} \rightarrow \gamma D_s^+$ and $D_s^{*+} \rightarrow \pi^0 D_s^+$ [2], is 1.0%. For the π^0 in the $D_s^+ \rightarrow \tau_\rho^+ \nu_\tau$, the systematic uncertainty is assigned to be 1.1% from the study of Ref. [16]. After reweighting by the individual signal yields, the systematic uncertainty due to the π^0 in the $D_s^+ \rightarrow \tau_\rho^+ \nu_\tau$ for the overall BF measurement of $D_s^+ \rightarrow \tau^+ \nu_\tau$ is 0.29%.

4. $E_{\text{sum}}^{\text{extra}\gamma}$ and $N_{\text{extra}}^{\text{charge}}$ requirements

The efficiency for the requirements on $E_{\text{sum}}^{\text{extra}\gamma}$ and $N_{\text{extra}}^{\text{charge}}$ is investigated with the double-tag sample of $D_s^+ \rightarrow \eta\pi^+$. The ratio of the averaged efficiency of data to that of simulation is 1.058 ± 0.022 . After multiplying the signal efficiency by this factor, we assign 2.2% as the systematic uncertainty. Reweighting by individual signal yields, the systematic uncertainty due to $E_{\text{sum}}^{\text{extra}\gamma}$ and $N_{\text{extra}}^{\text{charge}}$ requirements for the measurement of $D_s^+ \rightarrow \tau^+ \nu_\tau$ is 0.56%.

5. Tag bias

The single-tag efficiencies obtained from the inclusive MC sample differ from those estimated with the signal MC events generated with events containing the single-tag D_s^{*-} and signal decays, an effect known as ‘‘tag bias.’’ To estimate the MC simulation for these differences, we use a method from Ref. [39]. To study the tag bias, we assign 1.0% for the tracking and PID efficiencies of π^+ and K^+ , and 2.0% for π^0 , K_S^0 , $\eta(\gamma\gamma)$ reconstruction efficiencies of the tag side for their corresponding data and MC differences.

The difference from 1 of $\epsilon_{\text{ST}}^{D_s^+ \rightarrow \mu_a^+ \nu_\mu} / \epsilon_{\text{ST}}^{\text{inclusive } D_s^+}$ is assumed to not cancel in the BF measurements. Weighting the offsets in each tag mode by their relative single-tag yield, the average offset for $D_s^+ \rightarrow \mu_a^+ \nu_\mu$ is calculated to be $(1.28 \pm 0.01)\%$, which is taken as the systematic uncertainty.

Similarly, the systematic uncertainties due to tag bias are assigned as 1.19%, 1.28%, 1.22%, 1.19%, and 0.68% for $D_s^+ \rightarrow \mu_b^+ \nu_\mu$, $D_s^+ \rightarrow \tau_e^+ \nu_\tau$, $D_s^+ \rightarrow \tau_\mu^+ \nu_\tau$, $D_s^+ \rightarrow \tau_\pi^+ \nu_\tau$, and $D_s^+ \rightarrow \tau_\rho^+ \nu_\tau$, respectively. Reweighting by individual signal yields, the systematic uncertainty due to tag bias for the measurement of the BF of $D_s^+ \rightarrow \tau^+ \nu_\tau$ is 1.16%.

6. MC statistics

The uncertainties due to the MC statistics are assigned to be 0.40%, 0.51%, 0.29%, 0.40%, and 0.32% for $D_s^+ \rightarrow \mu^+ \nu_\mu$, $D_s^+ \rightarrow \tau_e^+ \nu_\tau$, $D_s^+ \rightarrow \tau_\mu^+ \nu_\tau$, $D_s^+ \rightarrow \tau_\pi^+ \nu_\tau$, and $D_s^+ \rightarrow \tau_\rho^+ \nu_\tau$, respectively. Reweighting by individual signal yields, the systematic uncertainty due to MC statistics for the measurement of the BF of $D_s^+ \rightarrow \tau^+ \nu_\tau$ is 0.25%.

7. M_{miss}^2 and $E_{\text{sum}}^{\text{extra}\gamma}$ fit

The uncertainties in the M_{miss}^2 and $E_{\text{sum}}^{\text{extra}\gamma}$ fits arise from the signal and background shapes.

For $D_s^+ \rightarrow \mu_a^+ \nu_\mu$, the systematic uncertainty due to the signal shape is estimated by replacing the nominal shape with signal shape convolved with a double Gaussian function with floating parameters. The relative change between the remeasured and nominal BF, 1.12%, is taken as the systematic uncertainty. For $D_s^+ \rightarrow \tau_\mu^+ \nu_\tau$ and $D_s^+ \rightarrow \tau_e^+ \nu_\tau$, we use the MC-simulated shapes convolved with a single Gaussian resolution function with free parameters. For $D_s^+ \rightarrow \mu_b^+ \nu_\mu$, $D_s^+ \rightarrow \tau_\pi^+ \nu_\tau$, and $D_s^+ \rightarrow \tau_\rho^+ \nu_\tau$, the systematic uncertainty due to the signal shape is estimated by replacing the nominal shape by varying the Gaussian shape parameters individually by $\pm 1\sigma$. The quadrature sum of the relative changes between the remeasured BFs and the nominal BF, 0.60%, is assigned as the systematic uncertainty for $D_s^+ \rightarrow \tau^+ \nu_\tau$.

For $D_s^+ \rightarrow \mu_a^+ \nu_\mu$, the peaking background is mainly due to the misidentification of a π^+ or a K^+ as a μ^+ . We have corrected the background yields considering the data-MC differences. The systematic uncertainty is assigned by varying the weights of various background sources within $\pm 1\sigma$ of individual BFs. We also try alternative MC-simulated shapes by varying the relative fractions of the main backgrounds from $D_s^\pm D_s^{*\mp}$, $D_s^* D_s^{*+}$, and $q\bar{q}$ by $\pm 1\sigma$ according to the observed cross sections, following Refs. [34,40]. After considering the uncertainties of the correction factors and changing the weights of different background shapes according to their yield uncertainties, we assign 0.80% as the associated systematic uncertainty.

To study the systematic uncertainty caused by the background shape in the fit for the measurement of $D_s^+ \rightarrow \tau^+ \nu_\tau$, we remeasure the BF by varying the background models in three ways. First, we use alternative MC-simulated shapes obtained by varying the relative fractions of the main backgrounds from $D_s^\pm D_s^{*\mp}$, $D_s^* D_s^{*+}$ and $q\bar{q}$. We vary background yield by $\pm 1\sigma$ according to the observed cross sections [40,34]. Second, we try alternative MC-simulated shapes obtained by varying the relative fractions of their largest background sources. Third, we vary the yields of the main background sources by varying $\pm 1\sigma$ of the quoted BFs. Finally, we assign 2.34% as the systematic uncertainty in the measurement of the BF of $D_s^+ \rightarrow \tau^+ \nu_\tau$.

8. Quoted branching fractions

The BFs of $\tau^+ \rightarrow \mu^+ \nu_\mu \bar{\nu}_\tau$, $\tau^+ \rightarrow e^+ \nu_e \bar{\nu}_\tau$, $\tau^+ \rightarrow \pi^+ \bar{\nu}_\tau$, and $\tau^+ \rightarrow \rho^+ \bar{\nu}_\tau$ are quoted from the PDG [2], which are $(17.39 \pm 0.04)\%$, $(17.82 \pm 0.04)\%$, $(10.82 \pm 0.05)\%$, and $(25.49 \pm 0.09)\%$, with relative uncertainties of 0.23%, 0.22%, 0.46%, and 0.35%, respectively. After reweighting these by the individual signal yields, the systematic uncertainty for the BF of $D_s^+ \rightarrow \tau^+ \nu_\tau$ is assigned as 0.14%.

The BFs of $D_s^{*+} \rightarrow \gamma D_s^+$ and $D_s^{*+} \rightarrow \pi^0 D_s^+$ are $(93.5 \pm 0.7)\%$ and $(5.8 \pm 0.7)\%$ [2]. By varying the BFs by these uncertainties, we find that the signal efficiencies change by no more than 0.30%, which is assigned as a systematic uncertainty. The effect of the BF uncertainty on $D_s^{*+} \rightarrow e^+ e^- D_s^+$ is negligible.

The total systematic uncertainties for the quoted BFs in the BF measurements of $D_s^+ \rightarrow \mu^+ \nu_\mu$ and $D_s^+ \rightarrow \tau^+ \nu_\tau$ are 0.30% and 0.33%, respectively.

B. Total systematic uncertainties without lepton universality constraint

Table VI summarizes all systematic uncertainties in the measurements of the BFs of $D_s^+ \rightarrow \mu_a^+ \nu_\mu$, $D_s^+ \rightarrow \mu_b^+ \nu_\mu$, and $D_s^+ \rightarrow \tau^+ \nu_\tau$. Assuming that all systematic uncertainties are independent with each other, the total systematic uncertainties in the measurements of the BFs of $D_s^+ \rightarrow \mu_a^+ \nu_\mu$, $D_s^+ \rightarrow \mu_b^+ \nu_\mu$, and $D_s^+ \rightarrow \tau^+ \nu_\tau$ are obtained by summing in quadrature, giving 2.88%, 4.13%, and 3.59%, respectively.

C. Total systematic uncertainty with lepton universality constraint

When constraining the yields of $D_s^+ \rightarrow \mu^+ \nu_\mu$ and $D_s^+ \rightarrow \tau^+ \nu_\tau$, the uncertainties of N_{ST} and quoted BFs are fully correlated and all other uncertainties are independent. For the independent system uncertainties, we vary the signal efficiency of the corresponding uncertainties $\pm 1\sigma$ to obtain the new BF measurement. The systematic uncertainty due to lepton universality constraint is assigned to be 0.04% by varying the fixed R within $\pm 1\sigma$. We assign the relative change of the BF as the corresponding uncertainty. Table VI summarizes the systematic uncertainties for individual sources. The total systematic uncertainty in the measurement of the BFs of $D_s^+ \rightarrow \ell^+ \nu_\ell$ (SM) is the quadrature sum which gives 3.74%.

VII. CONCLUSION

By analyzing 10.64 fb⁻¹ of $e^+ e^-$ collision data taken at $E_{\text{c.m.}}$ between 4.237 and 4.699 GeV with the BESIII detector, the BFs of $D_s^+ \rightarrow \mu^+ \nu_\mu$ and $D_s^+ \rightarrow \tau^+ \nu_\tau$ are determined with and without constraining the ratios of their BFs to the SM prediction. The obtained BFs are shown in Table IV. Combining these BFs with the world averages of the masses of ℓ^+ and D_s^+ as well as the lifetime of D_s^+ , we obtain $f_{D_s^+} |V_{cs}|$ with Eq. (1). The comparisons of the BFs and $f_{D_s^+} |V_{cs}|$ obtained in this work and the other measurements are shown in Table VII.

With the BFs of $D_s^+ \rightarrow \mu^+ \nu_\mu$ and $D_s^+ \rightarrow \tau^+ \nu_\tau$ without the SM constraint, we determine the ratio of the two decay widths to be $\frac{\Gamma_{D_s^+ \rightarrow \tau^+ \nu_\tau}}{\Gamma_{D_s^+ \rightarrow \mu^+ \nu_\mu}} = 10.24 \pm 0.57$. It is consistent with the SM prediction of 9.75 within 0.9σ , implying no violation of $\tau - \mu$ lepton-flavor universality. Taking the

TABLE VII. Comparisons of the BFs and the corresponding products of $f_{D_s^+}|V_{cs}|$ from various experiments. The “weighted” values are obtained by combining results after considering the correlated effects. The “average” values are obtained by weighting both statistical and systematic uncertainties, but not the third uncertainty dominated by the uncertainty of the D_s^+ lifetime. The uncertainties of average BFs and the first uncertainties of average $f_{D_s^+}|V_{cs}|$ are the total experimental uncertainties combined from statistical and systematic effects, and the second uncertainties of average $f_{D_s^+}|V_{cs}|$ is due to the input uncertainty of the quoted lifetime of D_s^+ . All weighted and average results do not include results constrained by the SM.

| Experiment | $E_{c.m.}$ (GeV) | Mode | D_s^+ decay | \mathcal{B} (%) | $f_{D_s^+} V_{cs} $ (MeV) |
|-----------------------|------------------|------------------------|---|---------------------------------|-----------------------------------|
| This work | 4.237–4.699 | $D_s^{*\pm}D_s^{*\mp}$ | $\tau_e^+\nu_\tau, \tau_\mu^+\nu_\tau, \tau_\pi^+\nu_\tau, \tau_\rho^+\nu_\tau$ | $5.60 \pm 0.16 \pm 0.20$ | $252.7 \pm 3.6 \pm 4.5 \pm 0.6$ |
| This work (SM) | 4.237–4.699 | $D_s^{*\pm}D_s^{*\mp}$ | $\tau_e^+\nu_\tau, \tau_\mu^+\nu_\tau, \tau_\pi^+\nu_\tau, \tau_\rho^+\nu_\tau$ | $5.39 \pm 0.14 \pm 0.20$ | $247.9 \pm 3.2 \pm 4.6 \pm 0.5$ |
| BESIII [14] | 4.009 | $D_s^+D_s^-$ | $\tau_\pi^+\nu_\tau$ | $3.28 \pm 1.83 \pm 0.37$ | $193.4 \pm 53.9 \pm 10.9 \pm 0.5$ |
| BESIII [16] | 4.178–4.226 | $D_s^\pm D_s^{*\mp}$ | $\tau_\rho^+\nu_\tau$ | $5.30 \pm 0.25 \pm 0.20$ | $245.8 \pm 5.8 \pm 4.6 \pm 0.5$ |
| BESIII [17] | 4.178–4.226 | $D_s^\pm D_s^{*\mp}$ | $\tau_\pi^+\nu_\tau$ | $5.21 \pm 0.25 \pm 0.17$ | $243.7 \pm 5.8 \pm 4.0 \pm 0.5$ |
| BESIII [18] | 4.178–4.226 | $D_s^\pm D_s^{*\mp}$ | $\tau_e^+\nu_\tau$ | $5.27 \pm 0.10 \pm 0.13$ | $245.1 \pm 2.3 \pm 3.0 \pm 0.5$ |
| BESIII [19] | 4.128–4.226 | $D_s^\pm D_s^{*\mp}$ | $\tau_\pi^+\bar{\nu}_\tau$ | $5.44 \pm 0.17 \pm 0.13$ | $249.0 \pm 3.9 \pm 3.0 \pm 0.5$ |
| BESIII [20] | 4.128–4.226 | $D_s^\pm D_s^{*\mp}$ | $\tau_\mu^+\bar{\nu}_\tau$ | $5.37 \pm 0.17 \pm 0.15$ | $247.4 \pm 3.9 \pm 3.5 \pm 0.5$ |
| Weighted ^a | ... | ... | $\tau^+\nu_\tau$ | $5.359 \pm 0.067 \pm 0.075$ | $247.2 \pm 1.5 \pm 1.7 \pm 0.5$ |
| CLEO [9] | 4.170 | $D_s^\pm D_s^{*\mp}$ | $\tau_e^+\nu_\tau$ | $5.30 \pm 0.47 \pm 0.22$ | $245.8 \pm 10.9 \pm 5.1 \pm 0.5$ |
| CLEO [10] | 4.170 | $D_s^\pm D_s^{*\mp}$ | $\tau_\rho^+\nu_\tau$ | $5.52 \pm 0.57 \pm 0.21$ | $250.9 \pm 13.0 \pm 4.8 \pm 0.6$ |
| CLEO [11] | 4.170 | $D_s^\pm D_s^{*\mp}$ | $\tau_\pi^+\nu_\tau$ | $6.42 \pm 0.81 \pm 0.18$ | $270.5 \pm 17.1 \pm 3.8 \pm 0.6$ |
| BABAR [12] | 10.56 | $DKX\gamma D_s^-$ | $\tau_e^+\nu_\tau, \tau_\mu^+\nu_\tau$ | $4.96 \pm 0.37 \pm 0.57$ | $237.8 \pm 8.9 \pm 13.7 \pm 0.5$ |
| Belle [13] | 10.56 | $DKX\gamma D_s^-$ | $\tau_\pi^+\nu_\tau, \tau_e^+\nu_\tau, \tau_\mu^+\nu_\tau$ | $5.70 \pm 0.21^{+0.31}_{-0.30}$ | $254.9 \pm 4.7 \pm 7.0 \pm 0.6$ |
| Average | | | | 5.38 ± 0.09 | $247.7 \pm 2.1 \pm 0.5$ |
| This work | 4.237–4.699 | $D_s^{*\pm}D_s^{*\mp}$ | $\mu^+\nu_\mu$ | $0.547 \pm 0.026 \pm 0.016$ | $246.5 \pm 5.9 \pm 3.6 \pm 0.5$ |
| This work (SM) | 4.237–4.699 | $D_s^{*\pm}D_s^{*\mp}$ | $\mu^+\nu_\mu$ | $0.553 \pm 0.014 \pm 0.020$ | ... |
| BESIII [14] | 4.009 | $D_s^+D_s^-$ | $\mu^+\nu_\mu$ | $0.517 \pm 0.075 \pm 0.021$ | $239.6 \pm 17.4 \pm 4.9 \pm 0.5$ |
| BESIII [15] | 4.178 | $D_s^\pm D_s^{*\mp}$ | $\mu^+\nu_\mu$ | $0.549 \pm 0.016 \pm 0.015$ | $246.9 \pm 3.6 \pm 3.4 \pm 0.5$ |
| BESIII [17] | 4.178–4.226 | $D_s^\pm D_s^{*\mp}$ | $\mu^+\nu_\mu$ | $0.535 \pm 0.013 \pm 0.016$ | $243.7 \pm 3.0 \pm 3.6 \pm 0.5$ |
| BESIII [21] | 4.128–4.226 | $D_s^\pm D_s^{*\mp}$ | $\mu^+\nu_\mu$ | $0.5294 \pm 0.0108 \pm 0.0085$ | $242.5 \pm 2.5 \pm 1.9 \pm 0.5$ |
| Weighted ^b | ... | ... | $\mu^+\nu_\mu$ | $0.5310 \pm 0.0099 \pm 0.0053$ | $242.8 \pm 2.3 \pm 1.2 \pm 0.5$ |
| Weighted ^c | ... | ... | $\tau^+\nu_\tau, \mu^+\nu_\mu$ | ... | $245.4 \pm 1.3 \pm 1.7 \pm 0.5$ |
| CLEO [11] | 4.170 | $D_s^\pm D_s^{*\mp}$ | $\mu^+\nu_\mu$ | $0.565 \pm 0.045 \pm 0.017$ | $250.5 \pm 10.0 \pm 3.8 \pm 0.5$ |
| BABAR [12] | 10.56 | $DKX\gamma D_s^-$ | $\mu^+\nu_\mu$ | $0.602 \pm 0.038 \pm 0.034$ | $258.6 \pm 8.2 \pm 7.3 \pm 0.5$ |
| Belle [13] | 10.56 | $DKX\gamma D_s^-$ | $\mu^+\nu_\mu$ | $0.531 \pm 0.028 \pm 0.020$ | $242.8 \pm 6.4 \pm 4.6 \pm 0.5$ |
| Average | | | | 0.539 ± 0.009 | $244.6 \pm 2.0 \pm 0.5$ |

^aWeighted excludes BESIII [17].

^bWeighted excludes BESIII [15,17].

^cWeighted excludes BESIII [15,17].

CKM matrix element $|V_{cs}| = 0.97349 \pm 0.00016$ from the global SM fit [2], we obtain $f_{D_s^+} = (253.2 \pm 6.0_{\text{stat}} \pm 3.7_{\text{syst}} \pm 0.6_{\text{input}})_{\mu\nu}$ and $f_{D_s^+} = (259.6 \pm 3.7_{\text{stat}} \pm 4.6_{\text{syst}} \pm 0.6_{\text{input}})_{\tau\nu}$ MeV, which agree with the value from recent LQCD calculations [3] within 0.4σ and 1.6σ . Conversely, taking the averaged decay constant $f_{D_s^+} = (249.9 \pm 0.5)$ MeV from recent LQCD calculations [3], we obtain $|V_{cs}| = (0.986 \pm 0.023_{\text{stat}} \pm 0.014_{\text{syst}} \pm 0.003_{\text{input}})_{\mu\nu}$ and $|V_{cs}| = (1.011 \pm 0.014_{\text{stat}} \pm 0.018_{\text{syst}} \pm 0.003_{\text{input}})_{\tau\nu}$, which agree with the value from the global SM fit [2] within 0.4σ and 1.6σ . The $f_{D_s^+}$ values obtained in this work offer complementary data to test the LQCD calculations and the $|V_{cs}|$ measurements are important for CKM matrix unitarity tests.

The averaged BF of $D_s^+ \rightarrow \mu^+\nu_\mu$ is obtained by reweighting the results reported in Refs. [14,21] and the one in this work. The averaged BF of $D_s^+ \rightarrow \tau^+\nu_\tau$ is obtained by reweighting the results measured by using the decays $\tau^+ \rightarrow \pi^+\pi^0\bar{\nu}_\tau$ [16], $\tau^+ \rightarrow e^+\bar{\nu}_\tau\nu_e$ [18], $\tau^+ \rightarrow \mu^+\bar{\nu}_\tau\nu_\mu$ [20], $\tau^+ \rightarrow \pi^+\bar{\nu}_\tau$ [19], the one measured in this work, and Ref. [14]. Using the method described in [41] which takes into account the correlation of systematic uncertainties, we obtain the averaged BFs to be $\mathcal{B}_{D_s^+ \rightarrow \mu^+\nu_\mu} = (0.5310 \pm 0.0099_{\text{stat}} \pm 0.0053_{\text{syst}})\%$ and $\mathcal{B}_{D_s^+ \rightarrow \tau^+\nu_\tau} = (5.359 \pm 0.067_{\text{stat}} \pm 0.074_{\text{syst}})\%$. For $D_s^+ \rightarrow \mu^+\nu_\mu$, the single-tag yield, the π^+ tracking and PID, and the transition $\gamma(\pi^0)$ reconstruction are taken to be correlated; for $D_s^+ \rightarrow \tau^+\nu_\tau$, the uncertainties from the single-tag yield, the π^+ tracking

and PID, the transition $\gamma(\pi^0)$ reconstruction, the best $\gamma(\pi^0)$ selection, and the tag bias are taken to be correlated. Additional common uncertainties come from $\tau_{D_s^+}$, $m_{D_s^+}$, and $m_{\tau,\mu}$ for $f_{D_s^+}$ and $|V_{cs}|$, while all the other uncertainties are independent. We obtain $f_{D_s^+} = (249.4 \pm 2.3_{\text{stat}} \pm 1.2_{\text{syst}} \pm 0.5_{\text{input}})_{\mu\nu}$ and $f_{D_s^+} = (254.8 \pm 1.6_{\text{stat}} \pm 1.8_{\text{syst}} \pm 0.6_{\text{input}})_{\tau\nu}$ MeV, which agree with the value from recent LQCD calculations [3] within 0.3σ and 1.4σ . We also obtain $|V_{cs}| = (0.972 \pm 0.009_{\text{stat}} \pm 0.005_{\text{syst}} \pm 0.003_{\text{input}})_{\mu\nu}$ and $|V_{cs}| = (0.989 \pm 0.006_{\text{stat}} \pm 0.007_{\text{syst}} \pm 0.003_{\text{input}})_{\tau\nu}$, which agree with the value from the global SM fit [2] within 0.3σ and 1.5σ .

Furthermore, we reweight the two separate $f_{D_s^+}|V_{cs}|$ values from $D_s^+ \rightarrow \mu^+\nu_\mu$ and $D_s^+ \rightarrow \tau^+\nu_\tau$ mentioned above, under the assumption that the uncertainties from the single-tag yield, the π^+ tracking and PID, the e^+ tracking and PID, the μ^+ tracking and PID, the transition $\gamma(\pi^0)$ reconstruction, the best $\gamma(\pi^0)$ selection, and the tag bias are taken to be correlated. The common uncertainties come from $\tau_{D_s^+}$, $m_{D_s^+}$, and $m_{\tau,\mu}$ for $f_{D_s^+}$ and $|V_{cs}|$. Finally, we obtain $f_{D_s^+} = (252.1 \pm 1.3_{\text{stat}} \pm 1.7_{\text{syst}} \pm 0.5_{\text{input}})$ MeV, which agrees with the value from recent LQCD calculations [3] within 0.8σ , and $|V_{cs}| = 0.982 \pm 0.005_{\text{stat}} \pm 0.007_{\text{syst}} \pm 0.003_{\text{input}}$, which agrees with the value from the global SM fit [2] within 0.8σ .

ACKNOWLEDGMENTS

The BESIII Collaboration thanks the staff of BEPCII and the IHEP computing center for their strong support. This work is supported in part by National Key R&D

Program of China under Contracts No. 2023YFA1606000, No. 2023YFA1606704, No. 2020YFA0406300, No. 2020YFA0406400; National Natural Science Foundation of China (NSFC) under Contracts No. 12375092, No. 11635010, No. 11735014, No. 11935015, No. 11935016, No. 11935018, No. 11961141012, No. 12025502, No. 12035009, No. 12035013, No. 12061131003, No. 12192260, No. 12192261, No. 12192262, No. 12192263, No. 12192264, No. 12192265, No. 12221005, No. 12225509, No. 12235017; the Chinese Academy of Sciences (CAS) Large-Scale Scientific Facility Program; the CAS Center for Excellence in Particle Physics (CCEPP); Joint Large-Scale Scientific Facility Funds of the NSFC and CAS under Contract No. U1832207; 100 Talents Program of CAS; The Institute of Nuclear and Particle Physics (INPAC) and Shanghai Key Laboratory for Particle Physics and Cosmology; German Research Foundation DFG under Contracts No. 455635585, No. FOR5327, No. GRK 2149; Istituto Nazionale di Fisica Nucleare, Italy; Ministry of Development of Turkey under Contract No. DPT2006K-120470; National Research Foundation of Korea under Contract No. NRF-2022R1A2C1092335; National Science and Technology fund of Mongolia; National Science Research and Innovation Fund (NSRF) via the Program Management Unit for Human Resources and Institutional Development, Research and Innovation of Thailand under Contract No. B16F640076; Polish National Science Centre under Contract No. 2019/35/O/ST2/02907; The Swedish Research Council; U.S. Department of Energy under Contract No. DE-FG02-05ER41374.

APPENDIX: FITS TO THE M_{BC} DISTRIBUTIONS OF DATA SINGLE-TAG YIELDS IN DATA, SINGLE-TAG EFFICIENCIES, AND DOUBLE-TAG EFFICIENCIES AT OTHER ENERGY POINTS

Figures 4–13 show the fits to the M_{BC} distributions of ST D_s^{*-} candidates selected from data at the other energy points. Tables VIII–XVII show the single-tag yields in data, single-tag efficiencies, and double-tag efficiencies at the other energy points.

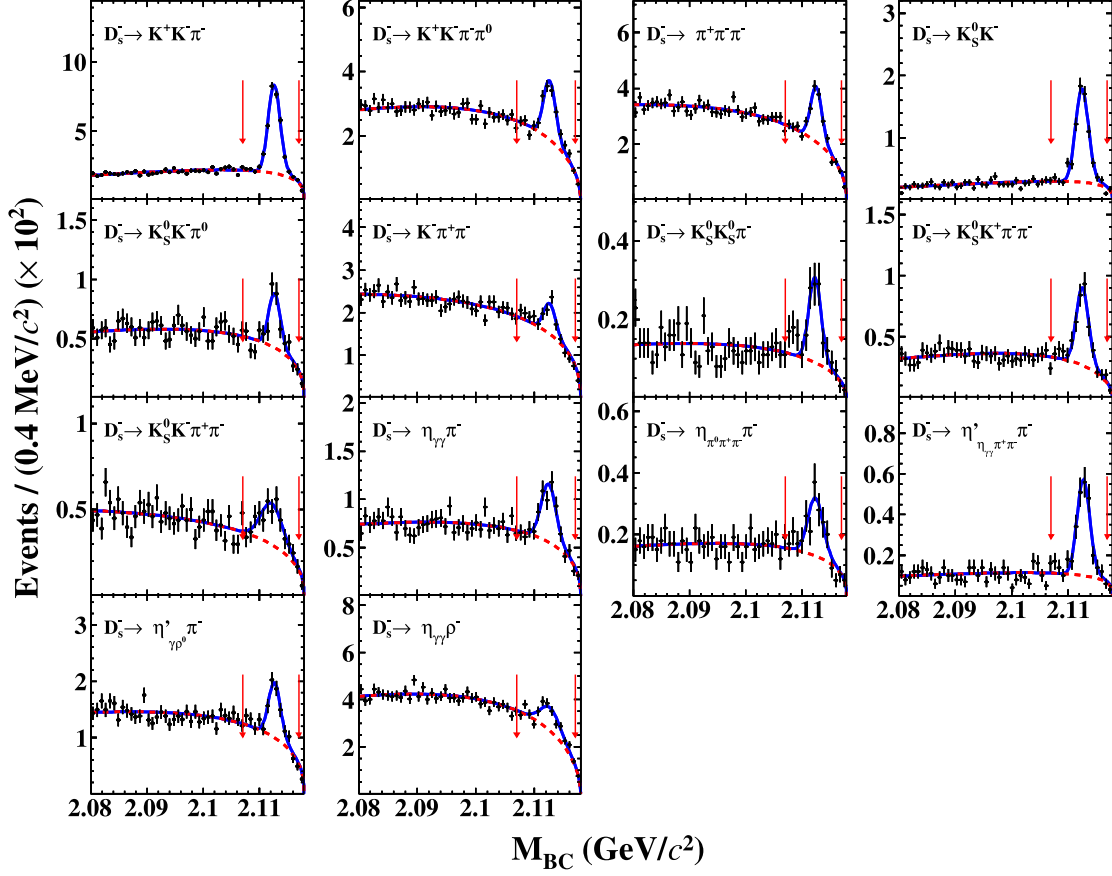


FIG. 4. Fits to the M_{BC} distributions of ST D_s^{*-} candidates selected from data at 4.237 GeV, where the points with error bars are data, the solid curves show the best fits, and the red dashed curves show the combinatorial background shapes. The pairs of arrows denote the M_{BC} signal window.

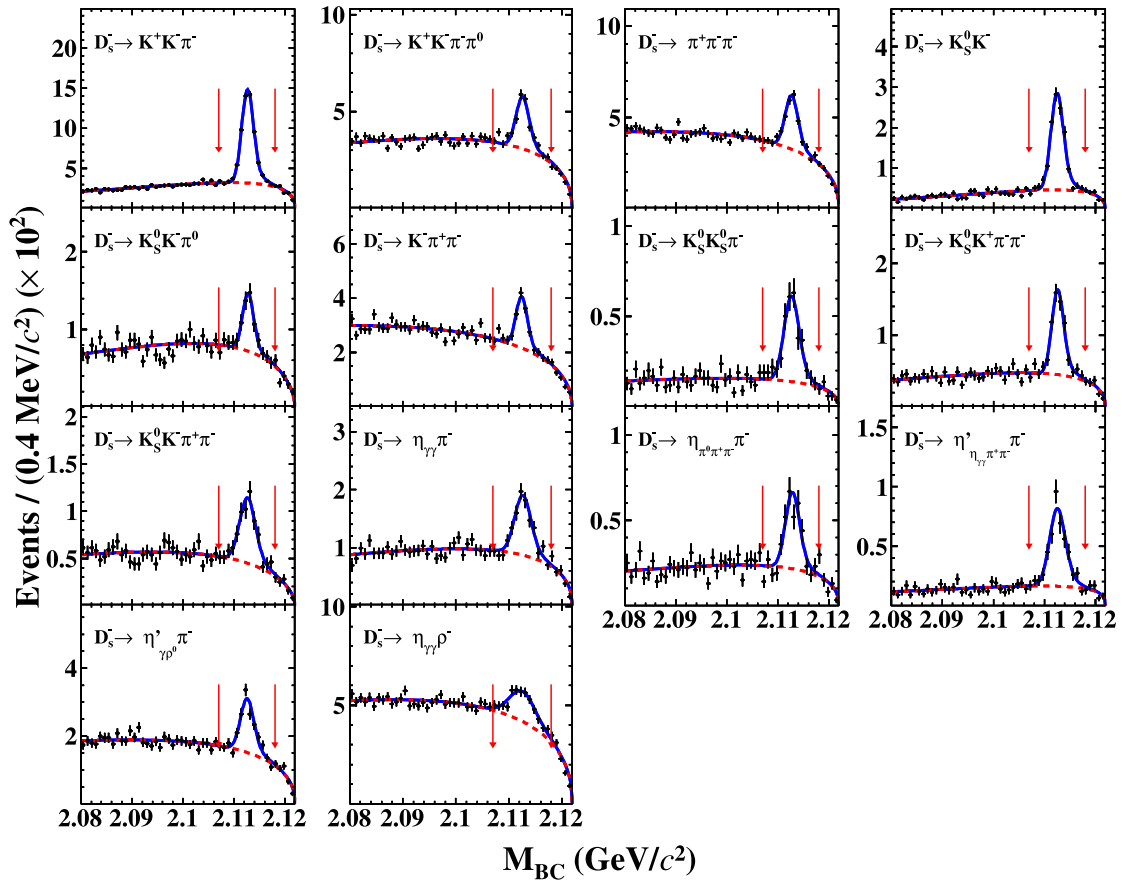


FIG. 5. Fits to the M_{BC} distributions of ST D_s^{*-} candidates selected from data at 4.246 GeV, where the points with error bars are data, the solid curves show the best fits, and the red dashed curves show the combinatorial background shapes. The pairs of arrows denote the M_{BC} signal window.

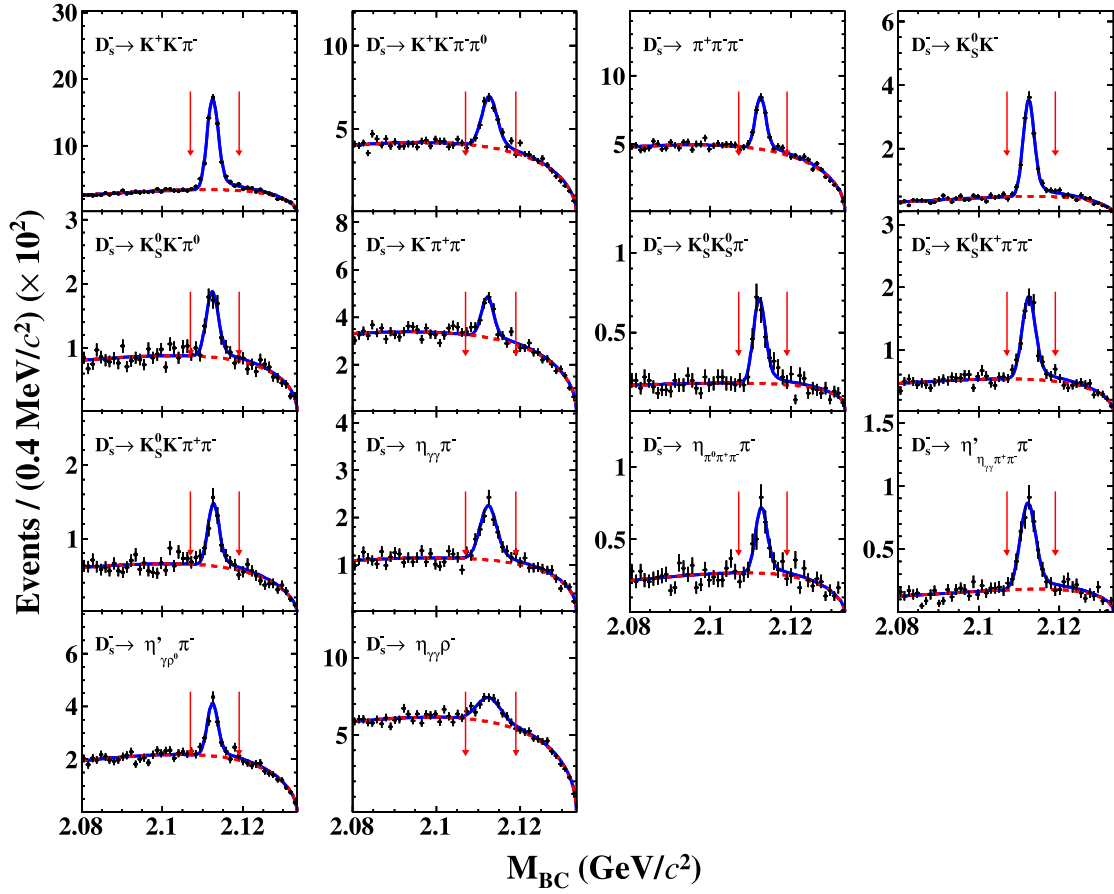


FIG. 6. Fits to the M_{BC} distributions of ST D_s^{*-} candidates selected from data at 4.270 GeV, where the points with error bars are data, the solid curves show the best fits, and the red dashed curves show the combinatorial background shapes. The pairs of arrows denote the M_{BC} signal window.

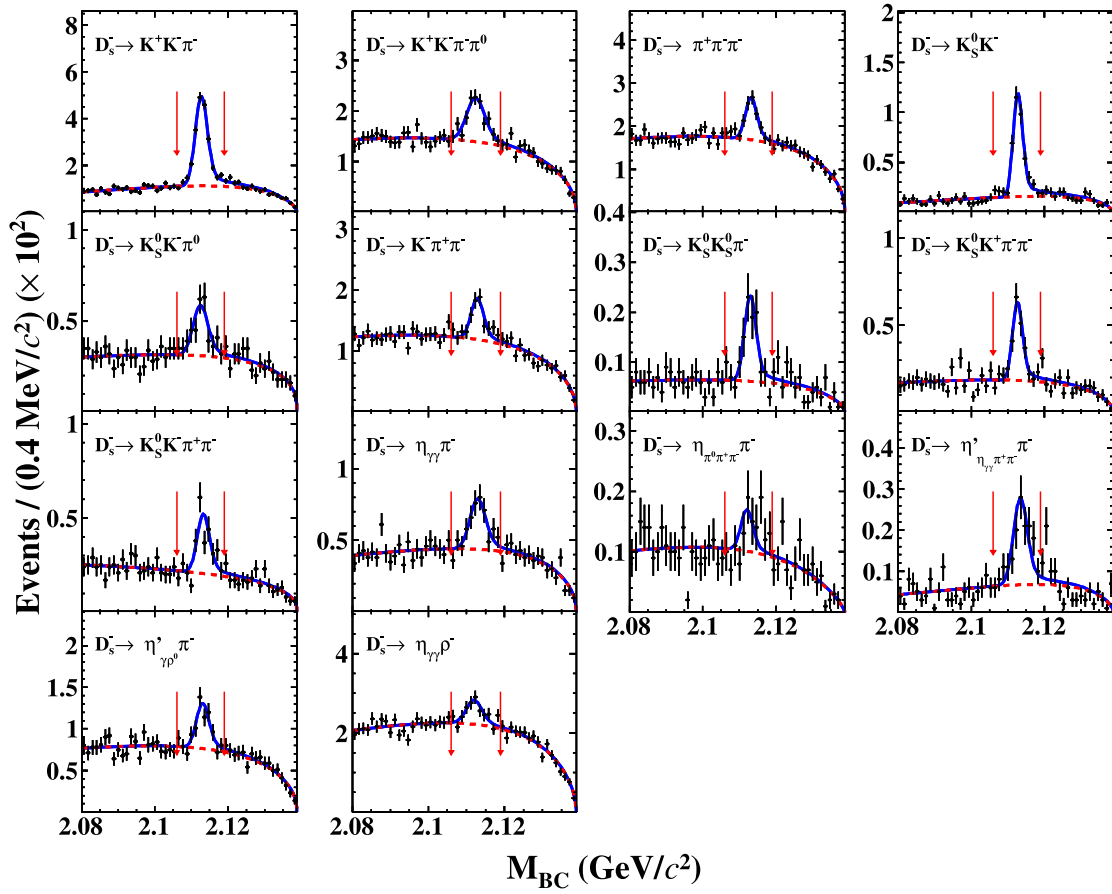


FIG. 7. Fits to the M_{BC} distributions of ST D_s^{*-} candidates selected from data at 4.280 GeV, where the points with error bars are data, the solid curves show the best fits, and the red dashed curves show the combinatorial background shapes. The pairs of arrows denote the M_{BC} signal window.

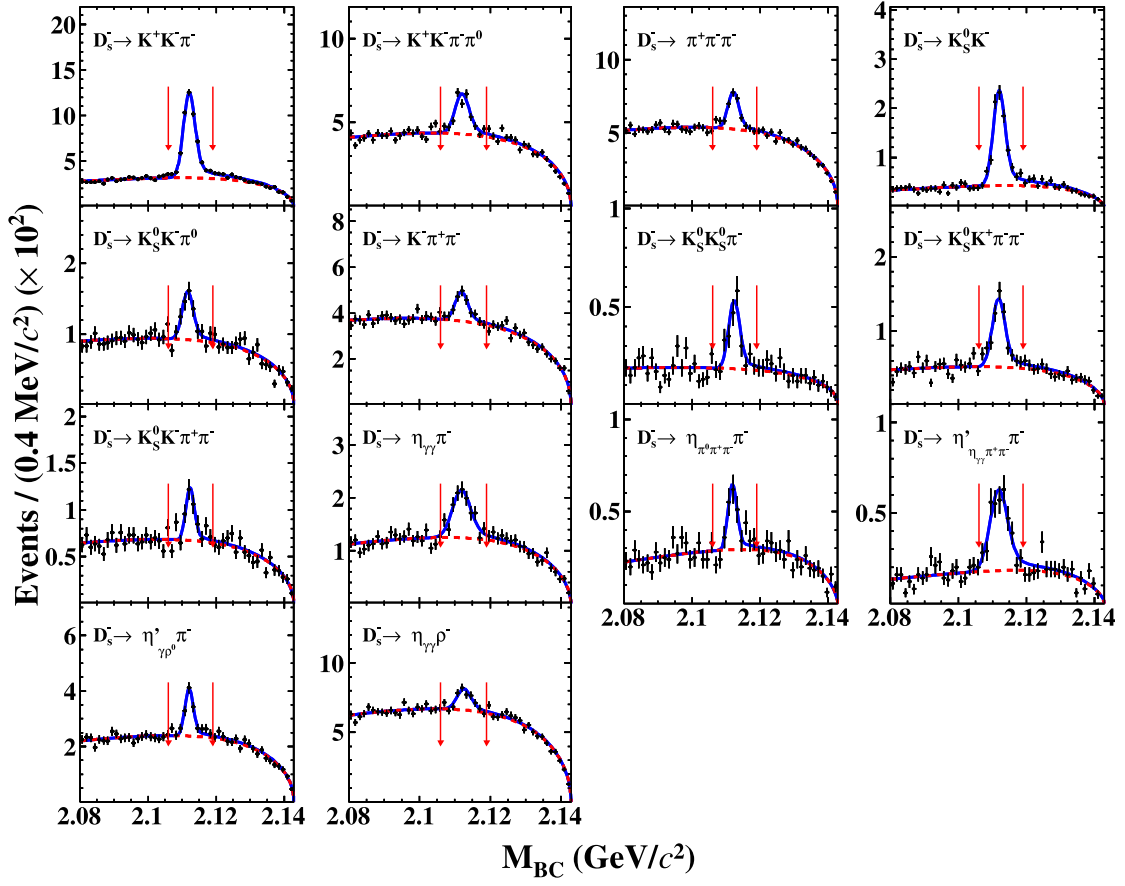


FIG. 8. Fits to the M_{BC} distributions of ST D_s^{*-} candidates selected from data at 4.290 GeV, where the points with error bars are data, the solid curves show the best fits, and the red dashed curves show the combinatorial background shapes. The pairs of arrows denote the M_{BC} signal window.

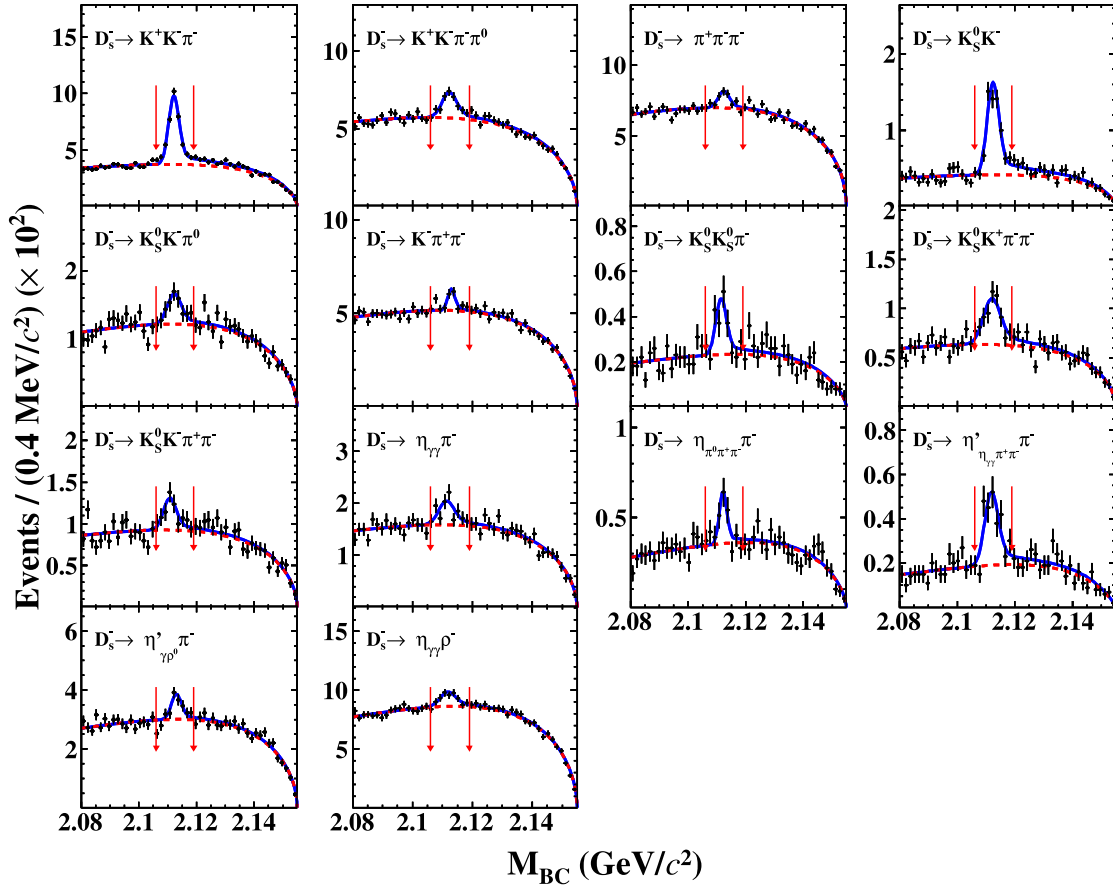


FIG. 9. Fits to the M_{BC} distributions of ST D_s^- candidates selected from data at 4.310–4.315 GeV, where the points with error bars are data, the solid curves show the best fits, and the red dashed curves show the combinatorial background shapes. The pairs of arrows denote the M_{BC} signal window.

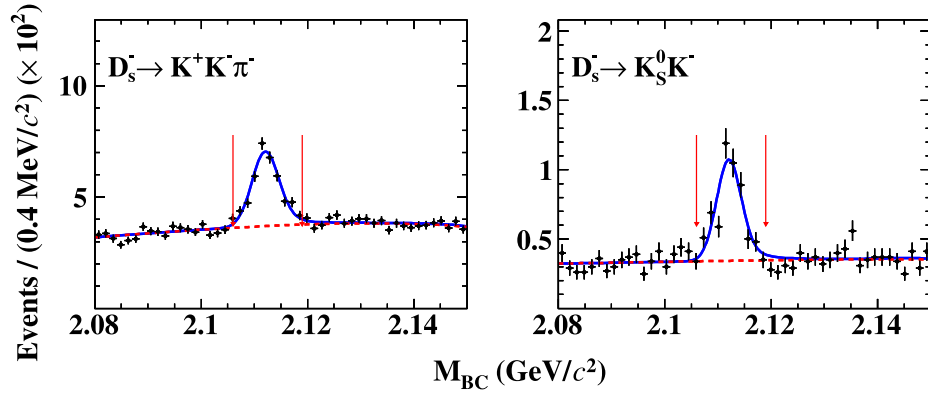


FIG. 10. Fits to the M_{BC} distributions of ST D_s^{*-} candidates selected from data at 4.400 GeV, where the points with error bars are data, the solid curves show the best fits, and the red dashed curves show the combinatorial background shapes. The pairs of arrows denote the M_{BC} signal window.

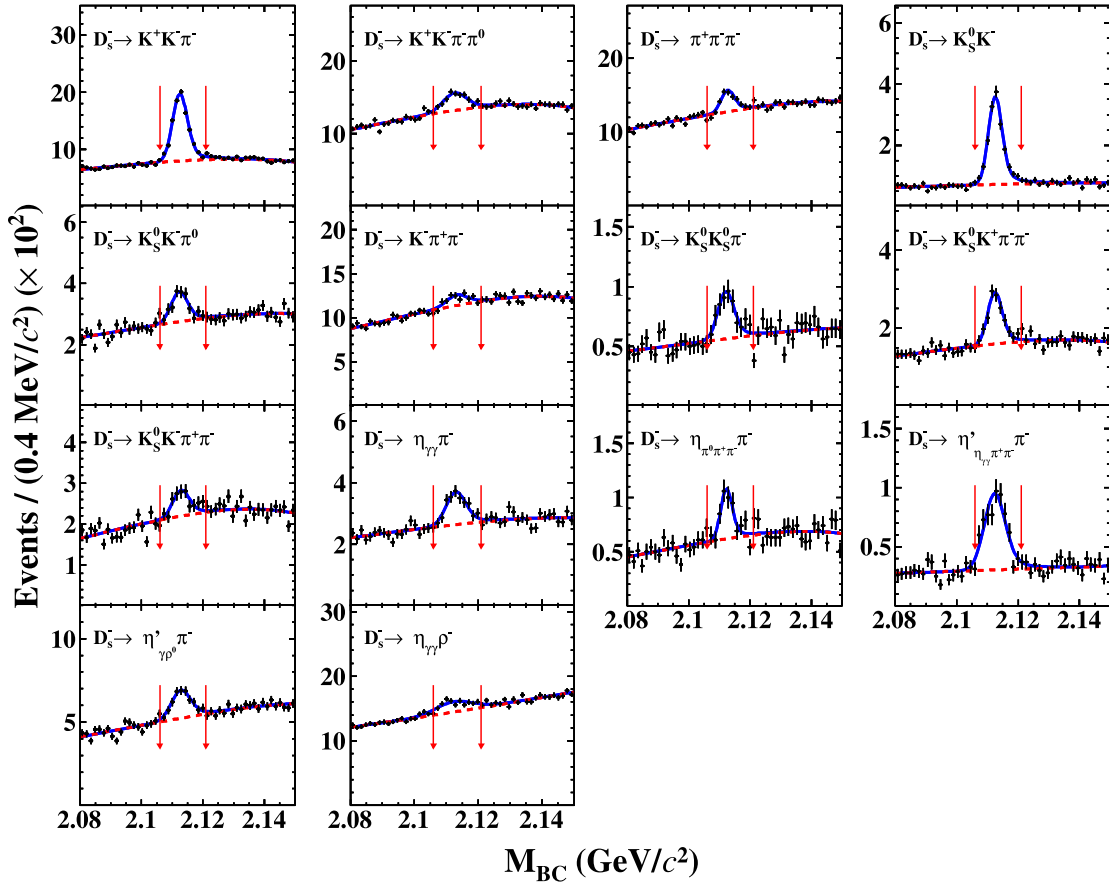


FIG. 11. Fits to the M_{BC} distributions of ST D_s^{*-} candidates selected from data at 4.420 GeV, where the points with error bars are data, the solid curves show the best fits, and the red dashed curves show the combinatorial background shapes. The pairs of arrows denote the M_{BC} signal window.

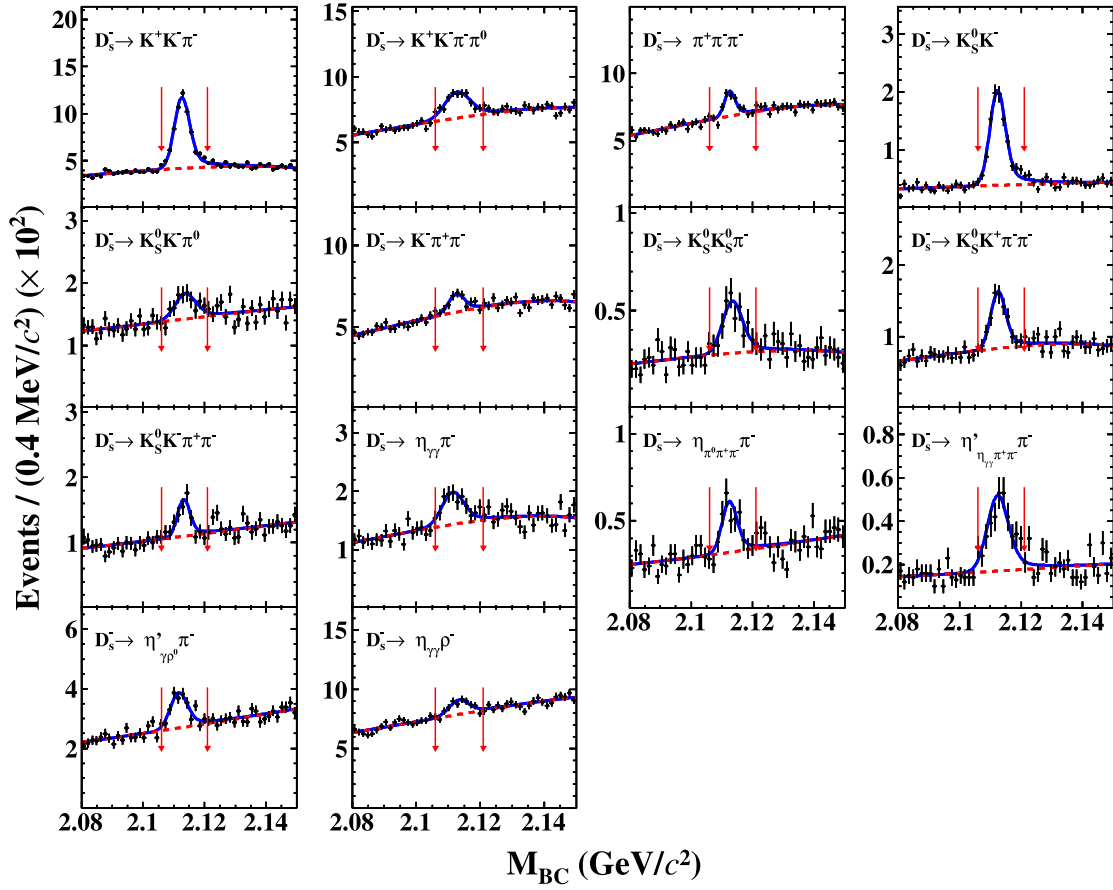


FIG. 12. Fits to the M_{BC} distributions of ST D_s^{*-} candidates selected from data at 4.440 GeV, where the points with error bars are data, the solid curves show the best fits, and the red dashed curves show the combinatorial background shapes. The pairs of arrows denote the M_{BC} signal window.

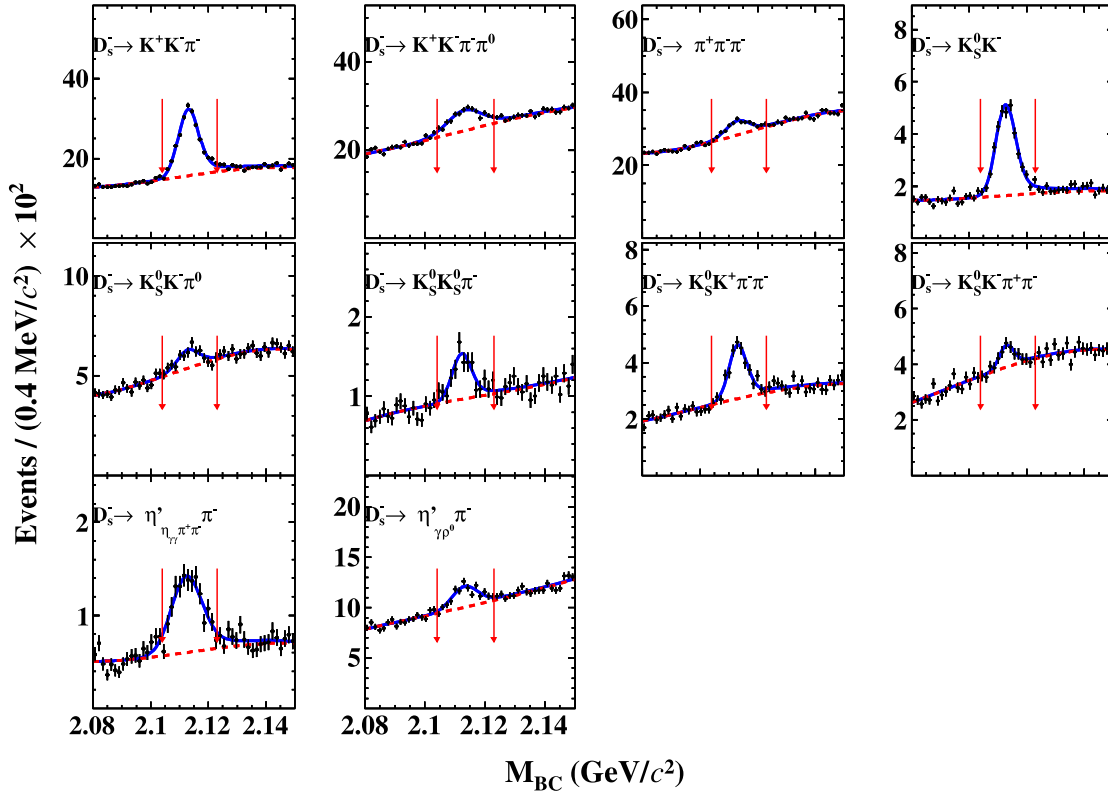


FIG. 13. Fits to the M_{BC} distributions of ST D_s^{*-} candidates selected from data at 4.470–4.699 GeV, where the points with error bars are data, the solid curves show the best fits, and the red dashed curves show the combinatorial background shapes. The pairs of arrows denote the M_{BC} signal window.

TABLE VIII. The single-tag yields (N_{ST}), single-tag efficiencies (ϵ_{ST}), and double-tag efficiencies for each tag mode at 4.237 GeV. The $\epsilon_{DT}^{\mu\nu}$ and $\epsilon_{DT}^{\mu\nu}$ correspond to the double-tag efficiencies for $D_s^+ \rightarrow \mu_a^+ \nu_\mu$ and $D_s^+ \rightarrow \mu_b^+ \nu_\mu$; the $\epsilon_{DT}^{\tau_e\nu}$, $\epsilon_{DT}^{\tau_\mu\nu}$, $\epsilon_{DT}^{\tau_\pi\nu}$, and $\epsilon_{DT}^{\tau_\rho\nu}$ correspond to the double-tag efficiencies for $D_s^+ \rightarrow \tau_c^+ \nu_\tau$, $D_s^+ \rightarrow \tau_\mu^+ \nu_\tau$, $D_s^+ \rightarrow \tau_\pi^+ \nu_\tau$, and $D_s^+ \rightarrow \tau_\rho^+ \nu_\tau$, respectively. The efficiencies include the BFs of D_s^{*+} and τ^+ decays. The uncertainties are statistical only.

| D_s^- tag mode | N_{ST} | ϵ_{ST} (%) | $\epsilon_{DT}^{\mu\nu}$ (%) | $\epsilon_{DT}^{\mu\nu}$ (%) | $\epsilon_{DT}^{\tau_e\nu}$ (%) | $\epsilon_{DT}^{\tau_\mu\nu}$ (%) | $\epsilon_{DT}^{\tau_\pi\nu}$ (%) | $\epsilon_{DT}^{\tau_\rho\nu}$ (%) |
|----------------------------------|---------------|---------------------|------------------------------|------------------------------|---------------------------------|-----------------------------------|-----------------------------------|------------------------------------|
| $K^+ K^- \pi^-$ | 2303 ± 72 | 20.47 ± 0.13 | 16.46 ± 0.08 | 17.98 ± 0.09 | 3.92 ± 0.02 | 1.83 ± 0.01 | 1.76 ± 0.01 | 1.17 ± 0.01 |
| $K^+ K^- \pi^- \pi^0$ | 635 ± 45 | 4.98 ± 0.10 | 5.57 ± 0.06 | 5.82 ± 0.07 | 1.37 ± 0.01 | 0.65 ± 0.01 | 0.58 ± 0.01 | 0.34 ± 0.01 |
| $\pi^- \pi^+ \pi^-$ | 675 ± 48 | 24.52 ± 0.48 | 20.53 ± 0.09 | 25.03 ± 0.10 | 4.71 ± 0.02 | 2.19 ± 0.01 | 2.49 ± 0.01 | 1.94 ± 0.02 |
| $K_S^0 K^-$ | 575 ± 34 | 24.04 ± 0.29 | 18.61 ± 0.10 | 22.51 ± 0.11 | 4.27 ± 0.02 | 1.97 ± 0.01 | 2.22 ± 0.01 | 1.71 ± 0.02 |
| $K_S^0 K^- \pi^0$ | 158 ± 25 | 8.58 ± 0.28 | 7.50 ± 0.10 | 9.16 ± 0.11 | 1.75 ± 0.02 | 0.84 ± 0.01 | 0.93 ± 0.01 | 0.61 ± 0.02 |
| $K^- \pi^- \pi^+$ | 247 ± 39 | 21.67 ± 0.65 | 18.38 ± 0.18 | 22.03 ± 0.20 | 4.25 ± 0.04 | 1.98 ± 0.03 | 2.19 ± 0.02 | 1.60 ± 0.03 |
| $K_S^0 K_S^0 \pi^-$ | 80 ± 21 | 11.44 ± 0.43 | 9.27 ± 0.16 | 11.47 ± 0.18 | 2.11 ± 0.03 | 0.96 ± 0.02 | 1.15 ± 0.02 | 0.72 ± 0.02 |
| $K_S^0 K^+ \pi^- \pi^-$ | 235 ± 28 | 10.51 ± 0.20 | 8.36 ± 0.13 | 9.89 ± 0.14 | 1.99 ± 0.03 | 0.93 ± 0.02 | 0.94 ± 0.01 | 0.60 ± 0.02 |
| $K_S^0 K^- \pi^+ \pi^-$ | 151 ± 39 | 9.89 ± 0.35 | 7.50 ± 0.07 | 8.60 ± 0.08 | 1.79 ± 0.01 | 0.84 ± 0.01 | 0.86 ± 0.01 | 0.54 ± 0.01 |
| $\eta_{\gamma\gamma} \pi^-$ | 257 ± 33 | 22.14 ± 0.59 | 19.05 ± 0.09 | 24.56 ± 0.10 | 4.27 ± 0.02 | 1.95 ± 0.01 | 2.46 ± 0.01 | 1.99 ± 0.02 |
| $\eta_{\pi^+ \pi^- \pi^0} \pi^-$ | 84 ± 19 | 10.96 ± 0.51 | 9.91 ± 0.08 | 12.48 ± 0.09 | 2.27 ± 0.01 | 1.06 ± 0.01 | 1.24 ± 0.01 | 0.89 ± 0.01 |
| $\eta' \pi^+ \pi^- \eta \pi^-$ | 179 ± 20 | 11.79 ± 0.32 | 10.06 ± 0.07 | 12.94 ± 0.08 | 2.27 ± 0.01 | 1.06 ± 0.01 | 1.29 ± 0.01 | 0.95 ± 0.01 |
| $\eta' \rho^0 \pi^-$ | 350 ± 47 | 15.44 ± 0.39 | 12.98 ± 0.07 | 16.46 ± 0.08 | 2.96 ± 0.01 | 1.39 ± 0.01 | 1.63 ± 0.01 | 1.12 ± 0.01 |
| $\eta_{\gamma\gamma} \rho^-$ | 548 ± 83 | 9.07 ± 0.27 | 9.31 ± 0.06 | 12.59 ± 0.07 | 2.12 ± 0.01 | 1.01 ± 0.01 | 1.29 ± 0.01 | 0.92 ± 0.01 |

TABLE IX. The single-tag yields (N_{ST}), single-tag efficiencies (ϵ_{ST}), and double-tag efficiencies for each tag mode at 4.246 GeV. The $\epsilon_{\text{DT}}^{\mu_a\nu}$ and $\epsilon_{\text{DT}}^{\mu_b\nu}$ correspond to the double-tag efficiencies for $D_s^+ \rightarrow \mu_a^+ \nu_\mu$ and $D_s^+ \rightarrow \mu_b^+ \nu_\mu$; the $\epsilon_{\text{DT}}^{\tau_e\nu}$, $\epsilon_{\text{DT}}^{\tau_\mu\nu}$, $\epsilon_{\text{DT}}^{\tau_\pi\nu}$, and $\epsilon_{\text{DT}}^{\tau_\rho\nu}$ correspond to the double-tag efficiencies for $D_s^+ \rightarrow \tau_e^+ \nu_\tau$, $D_s^+ \rightarrow \tau_\mu^+ \nu_\tau$, $D_s^+ \rightarrow \tau_\pi^+ \nu_\tau$, and $D_s^+ \rightarrow \tau_\rho^+ \nu_\tau$, respectively. The efficiencies include the BFs of D_s^{*+} and τ^+ decays. The uncertainties are statistical only.

| D_s^- tag mode | N_{ST} | ϵ_{ST} (%) | $\epsilon_{\text{DT}}^{\mu_a\nu}$ (%) | $\epsilon_{\text{DT}}^{\mu_b\nu}$ (%) | $\epsilon_{\text{DT}}^{\tau_e\nu}$ (%) | $\epsilon_{\text{DT}}^{\tau_\mu\nu}$ (%) | $\epsilon_{\text{DT}}^{\tau_\pi\nu}$ (%) | $\epsilon_{\text{DT}}^{\tau_\rho\nu}$ (%) |
|----------------------------------|-----------------|----------------------------|---------------------------------------|---------------------------------------|--|--|--|---|
| $K^+ K^- \pi^-$ | 4241 ± 94 | 20.11 ± 0.09 | 16.92 ± 0.08 | 17.49 ± 0.09 | 3.83 ± 0.02 | 1.78 ± 0.01 | 1.71 ± 0.01 | 1.14 ± 0.01 |
| $K^+ K^- \pi^- \pi^0$ | 1029 ± 81 | 5.39 ± 0.07 | 5.82 ± 0.06 | 5.64 ± 0.07 | 1.34 ± 0.01 | 0.63 ± 0.01 | 0.56 ± 0.01 | 0.32 ± 0.01 |
| $\pi^- \pi^+ \pi^-$ | 1149 ± 78 | 25.80 ± 0.34 | 20.65 ± 0.09 | 24.81 ± 0.10 | 4.59 ± 0.02 | 2.12 ± 0.01 | 2.45 ± 0.01 | 1.85 ± 0.02 |
| $K_S^0 K^-$ | 920 ± 41 | 23.66 ± 0.21 | 18.74 ± 0.10 | 22.02 ± 0.11 | 4.21 ± 0.02 | 1.95 ± 0.01 | 2.19 ± 0.01 | 1.67 ± 0.02 |
| $K_S^0 K^- \pi^0$ | 254 ± 31 | 7.89 ± 0.18 | 7.44 ± 0.10 | 8.90 ± 0.11 | 1.71 ± 0.02 | 0.78 ± 0.01 | 0.89 ± 0.01 | 0.60 ± 0.02 |
| $K^- \pi^- \pi^+$ | 634 ± 51 | 23.40 ± 0.52 | 18.59 ± 0.18 | 21.51 ± 0.20 | 4.16 ± 0.04 | 1.90 ± 0.03 | 2.15 ± 0.02 | 1.54 ± 0.03 |
| $K_S^0 K_S^0 \pi^-$ | 216 ± 23 | 11.21 ± 0.28 | 9.26 ± 0.16 | 11.10 ± 0.18 | 2.05 ± 0.03 | 0.96 ± 0.02 | 1.09 ± 0.02 | 0.76 ± 0.03 |
| $K_S^0 K^+ \pi^- \pi^-$ | 433 ± 33 | 10.08 ± 0.15 | 8.53 ± 0.13 | 9.36 ± 0.14 | 2.00 ± 0.03 | 0.90 ± 0.02 | 0.92 ± 0.01 | 0.59 ± 0.02 |
| $K_S^0 K^- \pi^+ \pi^-$ | 330 ± 35 | 9.07 ± 0.23 | 7.65 ± 0.07 | 8.44 ± 0.07 | 1.77 ± 0.01 | 0.84 ± 0.01 | 0.83 ± 0.01 | 0.53 ± 0.01 |
| $\eta_{\gamma\gamma} \pi^-$ | 492 ± 47 | 20.56 ± 0.40 | 18.65 ± 0.08 | 23.91 ± 0.10 | 4.15 ± 0.02 | 1.91 ± 0.01 | 2.39 ± 0.01 | 1.91 ± 0.02 |
| $\eta_{\pi^+ \pi^- \pi^0} \pi^-$ | 192 ± 22 | 10.92 ± 0.34 | 9.90 ± 0.07 | 12.42 ± 0.07 | 2.20 ± 0.01 | 1.02 ± 0.01 | 1.22 ± 0.01 | 0.86 ± 0.01 |
| $\eta'_{\pi^+ \pi^- \eta} \pi^-$ | 311 ± 27 | 11.35 ± 0.22 | 10.03 ± 0.07 | 12.82 ± 0.07 | 2.20 ± 0.01 | 1.03 ± 0.01 | 1.25 ± 0.01 | 0.91 ± 0.01 |
| $\eta'_{\gamma\rho} \pi^-$ | 650 ± 56 | 14.82 ± 0.25 | 12.70 ± 0.07 | 15.83 ± 0.08 | 2.89 ± 0.01 | 1.34 ± 0.01 | 1.56 ± 0.01 | 1.08 ± 0.01 |
| $\eta_{\gamma\gamma} \rho^-$ | 1093 ± 156 | 8.17 ± 0.17 | 9.02 ± 0.06 | 12.25 ± 0.07 | 2.04 ± 0.01 | 0.96 ± 0.01 | 1.24 ± 0.01 | 0.90 ± 0.01 |

TABLE X. The single-tag yields (N_{ST}), single-tag efficiencies (ϵ_{ST}), and double-tag efficiencies for each tag mode at 4.270 GeV. The $\epsilon_{\text{DT}}^{\mu_a\nu}$ and $\epsilon_{\text{DT}}^{\mu_b\nu}$ correspond to the double-tag efficiencies for $D_s^+ \rightarrow \mu_a^+ \nu_\mu$ and $D_s^+ \rightarrow \mu_b^+ \nu_\mu$; the $\epsilon_{\text{DT}}^{\tau_e\nu}$, $\epsilon_{\text{DT}}^{\tau_\mu\nu}$, $\epsilon_{\text{DT}}^{\tau_\pi\nu}$, and $\epsilon_{\text{DT}}^{\tau_\rho\nu}$ correspond to the double-tag efficiencies for $D_s^+ \rightarrow \tau_e^+ \nu_\tau$, $D_s^+ \rightarrow \tau_\mu^+ \nu_\tau$, $D_s^+ \rightarrow \tau_\pi^+ \nu_\tau$, and $D_s^+ \rightarrow \tau_\rho^+ \nu_\tau$, respectively. The efficiencies include the BFs of D_s^{*+} and τ^+ decays. The uncertainties are statistical only.

| D_s^- tag mode | N_{ST} | ϵ_{ST} (%) | $\epsilon_{\text{DT}}^{\mu_a\nu}$ (%) | $\epsilon_{\text{DT}}^{\mu_b\nu}$ (%) | $\epsilon_{\text{DT}}^{\tau_e\nu}$ (%) | $\epsilon_{\text{DT}}^{\tau_\mu\nu}$ (%) | $\epsilon_{\text{DT}}^{\tau_\pi\nu}$ (%) | $\epsilon_{\text{DT}}^{\tau_\rho\nu}$ (%) |
|----------------------------------|-----------------|----------------------------|---------------------------------------|---------------------------------------|--|--|--|---|
| $K^+ K^- \pi^-$ | 4822 ± 101 | 19.53 ± 0.09 | 15.48 ± 0.08 | 16.05 ± 0.08 | 3.49 ± 0.02 | 1.61 ± 0.01 | 1.60 ± 0.01 | 1.11 ± 0.01 |
| $K^+ K^- \pi^- \pi^0$ | 1368 ± 92 | 4.70 ± 0.06 | 5.25 ± 0.06 | 5.28 ± 0.06 | 1.18 ± 0.01 | 0.57 ± 0.01 | 0.51 ± 0.01 | 0.31 ± 0.01 |
| $\pi^- \pi^+ \pi^-$ | 1265 ± 81 | 25.40 ± 0.33 | 19.13 ± 0.09 | 22.82 ± 0.10 | 4.20 ± 0.02 | 1.95 ± 0.01 | 2.26 ± 0.01 | 1.76 ± 0.02 |
| $K_S^0 K^-$ | 1055 ± 44 | 23.09 ± 0.20 | 17.40 ± 0.10 | 20.55 ± 0.11 | 3.90 ± 0.02 | 1.77 ± 0.01 | 2.02 ± 0.01 | 1.59 ± 0.02 |
| $K_S^0 K^- \pi^0$ | 388 ± 40 | 7.74 ± 0.18 | 6.79 ± 0.10 | 8.34 ± 0.11 | 1.54 ± 0.02 | 0.73 ± 0.01 | 0.79 ± 0.01 | 0.56 ± 0.02 |
| $K^- \pi^- \pi^+$ | 618 ± 72 | 23.46 ± 0.56 | 17.21 ± 0.18 | 19.86 ± 0.19 | 3.81 ± 0.03 | 1.77 ± 0.02 | 1.94 ± 0.02 | 1.46 ± 0.03 |
| $K_S^0 K_S^0 \pi^-$ | 199 ± 23 | 10.98 ± 0.28 | 8.67 ± 0.16 | 10.70 ± 0.18 | 1.91 ± 0.03 | 0.89 ± 0.02 | 1.00 ± 0.02 | 0.72 ± 0.02 |
| $K_S^0 K^+ \pi^- \pi^-$ | 550 ± 39 | 10.08 ± 0.16 | 7.89 ± 0.12 | 8.73 ± 0.13 | 1.83 ± 0.03 | 0.82 ± 0.02 | 0.88 ± 0.01 | 0.57 ± 0.02 |
| $K_S^0 K^- \pi^+ \pi^-$ | 300 ± 36 | 9.40 ± 0.26 | 7.20 ± 0.07 | 7.97 ± 0.07 | 1.62 ± 0.01 | 0.77 ± 0.01 | 0.76 ± 0.01 | 0.52 ± 0.01 |
| $\eta_{\gamma\gamma} \pi^-$ | 557 ± 54 | 19.53 ± 0.41 | 16.79 ± 0.08 | 21.41 ± 0.09 | 3.72 ± 0.02 | 1.72 ± 0.01 | 2.13 ± 0.01 | 1.74 ± 0.01 |
| $\eta_{\pi^+ \pi^- \pi^0} \pi^-$ | 167 ± 24 | 10.59 ± 0.36 | 8.93 ± 0.06 | 11.06 ± 0.07 | 2.00 ± 0.01 | 0.93 ± 0.01 | 1.09 ± 0.01 | 0.78 ± 0.01 |
| $\eta'_{\pi^+ \pi^- \eta} \pi^-$ | 323 ± 27 | 10.91 ± 0.23 | 9.01 ± 0.06 | 11.48 ± 0.07 | 2.03 ± 0.01 | 0.92 ± 0.01 | 1.15 ± 0.01 | 0.85 ± 0.01 |
| $\eta'_{\gamma\rho} \pi^-$ | 674 ± 59 | 14.26 ± 0.27 | 11.58 ± 0.07 | 14.43 ± 0.08 | 2.62 ± 0.01 | 1.23 ± 0.01 | 1.42 ± 0.01 | 1.04 ± 0.01 |
| $\eta_{\gamma\gamma} \rho^-$ | 1033 ± 120 | 8.19 ± 0.18 | 7.93 ± 0.06 | 10.71 ± 0.07 | 1.79 ± 0.01 | 0.84 ± 0.01 | 1.11 ± 0.01 | 0.79 ± 0.01 |

TABLE XI. The single-tag yields (N_{ST}), single-tag efficiencies (ϵ_{ST}), and double-tag efficiencies for each tag mode at 4.280 GeV. The $\epsilon_{DT}^{\mu\nu}$ and $\epsilon_{DT}^{\mu b\nu}$ correspond to the double-tag efficiencies for $D_s^+ \rightarrow \mu_a^+ \nu_\mu$ and $D_s^+ \rightarrow \mu_b^+ \nu_\mu$; the $\epsilon_{DT}^{\tau_e\nu}$, $\epsilon_{DT}^{\tau_\mu\nu}$, $\epsilon_{DT}^{\tau_\pi\nu}$, and $\epsilon_{DT}^{\tau_\rho\nu}$ correspond to the double-tag efficiencies for $D_s^+ \rightarrow \tau_e^+ \nu_\tau$, $D_s^+ \rightarrow \tau_\mu^+ \nu_\tau$, $D_s^+ \rightarrow \tau_\pi^+ \nu_\tau$, and $D_s^+ \rightarrow \tau_\rho^+ \nu_\tau$, respectively. The efficiencies include the BFs of D_s^{*+} and τ^+ decays. The uncertainties are statistical only.

| D_s^- tag mode | N_{ST} | ϵ_{ST} (%) | $\epsilon_{DT}^{\mu a\nu}$ (%) | $\epsilon_{DT}^{\mu b\nu}$ (%) | $\epsilon_{DT}^{\tau_e\nu}$ (%) | $\epsilon_{DT}^{\tau_\mu\nu}$ (%) | $\epsilon_{DT}^{\tau_\pi\nu}$ (%) | $\epsilon_{DT}^{\tau_\rho\nu}$ (%) |
|----------------------------------|---------------|---------------------|--------------------------------|--------------------------------|---------------------------------|-----------------------------------|-----------------------------------|------------------------------------|
| $K^+ K^- \pi^-$ | 1467 ± 57 | 18.53 ± 0.15 | 15.08 ± 0.11 | 14.82 ± 0.11 | 3.34 ± 0.02 | 1.54 ± 0.02 | 1.43 ± 0.01 | 0.92 ± 0.02 |
| $K^+ K^- \pi^- \pi^0$ | 455 ± 63 | 5.27 ± 0.15 | 5.16 ± 0.09 | 4.74 ± 0.09 | 1.16 ± 0.02 | 0.57 ± 0.01 | 0.46 ± 0.01 | 0.23 ± 0.01 |
| $\pi^- \pi^+ \pi^-$ | 351 ± 50 | 24.06 ± 0.63 | 18.50 ± 0.12 | 21.53 ± 0.13 | 4.06 ± 0.02 | 1.86 ± 0.02 | 2.09 ± 0.01 | 1.45 ± 0.02 |
| $K_S^0 K^-$ | 310 ± 23 | 22.02 ± 0.35 | 16.73 ± 0.14 | 19.21 ± 0.15 | 3.68 ± 0.03 | 1.70 ± 0.02 | 1.81 ± 0.02 | 1.30 ± 0.02 |
| $K_S^0 K^- \pi^0$ | 125 ± 32 | 7.54 ± 0.34 | 6.69 ± 0.13 | 7.74 ± 0.15 | 1.47 ± 0.03 | 0.69 ± 0.02 | 0.77 ± 0.02 | 0.43 ± 0.02 |
| $K^- \pi^- \pi^+$ | 252 ± 54 | 23.16 ± 1.11 | 16.64 ± 0.25 | 18.32 ± 0.27 | 3.64 ± 0.05 | 1.69 ± 0.03 | 1.79 ± 0.03 | 1.21 ± 0.04 |
| $K_S^0 K_S^0 \pi^-$ | 61 ± 12 | 10.54 ± 0.49 | 7.97 ± 0.21 | 9.23 ± 0.23 | 1.80 ± 0.04 | 0.78 ± 0.03 | 0.85 ± 0.02 | 0.52 ± 0.03 |
| $K_S^0 K^+ \pi^- \pi^-$ | 141 ± 19 | 9.94 ± 0.28 | 7.86 ± 0.18 | 7.92 ± 0.18 | 1.69 ± 0.03 | 0.78 ± 0.02 | 0.75 ± 0.02 | 0.45 ± 0.02 |
| $K_S^0 K^- \pi^+ \pi^-$ | 119 ± 21 | 8.57 ± 0.43 | 6.78 ± 0.13 | 7.16 ± 0.14 | 1.52 ± 0.02 | 0.71 ± 0.01 | 0.68 ± 0.01 | 0.39 ± 0.01 |
| $\eta_{\gamma\gamma} \pi^-$ | 160 ± 32 | 17.49 ± 0.77 | 16.08 ± 0.11 | 20.53 ± 0.13 | 3.61 ± 0.02 | 1.68 ± 0.02 | 2.01 ± 0.01 | 1.47 ± 0.02 |
| $\eta_{\pi^+ \pi^- \pi^0} \pi^-$ | 26 ± 11 | 9.50 ± 0.55 | 8.73 ± 0.09 | 10.54 ± 0.10 | 1.88 ± 0.02 | 0.89 ± 0.01 | 1.02 ± 0.01 | 0.62 ± 0.01 |
| $\eta'_{\pi^+ \pi^- \eta} \pi^-$ | 98 ± 15 | 11.04 ± 0.39 | 8.77 ± 0.09 | 10.87 ± 0.10 | 1.94 ± 0.02 | 0.90 ± 0.01 | 1.07 ± 0.01 | 0.68 ± 0.01 |
| $\eta'_{\gamma\rho} \pi^-$ | 212 ± 34 | 11.29 ± 0.35 | 11.32 ± 0.10 | 13.75 ± 0.11 | 2.49 ± 0.02 | 1.21 ± 0.01 | 1.33 ± 0.01 | 0.83 ± 0.01 |
| $\eta_{\gamma\gamma} \rho^-$ | 286 ± 73 | 7.65 ± 0.39 | 7.75 ± 0.08 | 10.42 ± 0.10 | 1.71 ± 0.02 | 0.81 ± 0.01 | 1.01 ± 0.01 | 0.71 ± 0.01 |

TABLE XII. The single-tag yields (N_{ST}), single-tag efficiencies (ϵ_{ST}), and double-tag efficiencies for each tag mode at 4.290 GeV. The $\epsilon_{DT}^{\mu\nu}$ and $\epsilon_{DT}^{\mu b\nu}$ correspond to the double-tag efficiencies for $D_s^+ \rightarrow \mu_a^+ \nu_\mu$ and $D_s^+ \rightarrow \mu_b^+ \nu_\mu$; the $\epsilon_{DT}^{\tau_e\nu}$, $\epsilon_{DT}^{\tau_\mu\nu}$, $\epsilon_{DT}^{\tau_\pi\nu}$, and $\epsilon_{DT}^{\tau_\rho\nu}$ correspond to the double-tag efficiencies for $D_s^+ \rightarrow \tau_e^+ \nu_\tau$, $D_s^+ \rightarrow \tau_\mu^+ \nu_\tau$, $D_s^+ \rightarrow \tau_\pi^+ \nu_\tau$, and $D_s^+ \rightarrow \tau_\rho^+ \nu_\tau$, respectively. The efficiencies include the BFs of D_s^{*+} and τ^+ decays. The uncertainties are statistical only.

| D_s^- tag mode | N_{ST} | ϵ_{ST} (%) | $\epsilon_{DT}^{\mu a\nu}$ (%) | $\epsilon_{DT}^{\mu b\nu}$ (%) | $\epsilon_{DT}^{\tau_e\nu}$ (%) | $\epsilon_{DT}^{\tau_\mu\nu}$ (%) | $\epsilon_{DT}^{\tau_\pi\nu}$ (%) | $\epsilon_{DT}^{\tau_\rho\nu}$ (%) |
|----------------------------------|---------------|---------------------|--------------------------------|--------------------------------|---------------------------------|-----------------------------------|-----------------------------------|------------------------------------|
| $K^+ K^- \pi^-$ | 3432 ± 90 | 18.43 ± 0.09 | 14.34 ± 0.08 | 14.86 ± 0.08 | 3.22 ± 0.02 | 1.49 ± 0.01 | 1.40 ± 0.01 | 0.85 ± 0.01 |
| $K^+ K^- \pi^- \pi^0$ | 1018 ± 81 | 5.02 ± 0.09 | 4.86 ± 0.06 | 4.72 ± 0.06 | 1.09 ± 0.01 | 0.53 ± 0.01 | 0.44 ± 0.01 | 0.23 ± 0.01 |
| $\pi^- \pi^+ \pi^-$ | 869 ± 87 | 24.33 ± 0.42 | 18.09 ± 0.09 | 22.14 ± 0.10 | 4.00 ± 0.02 | 1.85 ± 0.01 | 2.11 ± 0.01 | 1.45 ± 0.01 |
| $K_S^0 K^-$ | 727 ± 39 | 21.35 ± 0.22 | 15.94 ± 0.10 | 19.07 ± 0.11 | 3.51 ± 0.02 | 1.63 ± 0.01 | 1.78 ± 0.01 | 1.24 ± 0.02 |
| $K_S^0 K^- \pi^0$ | 239 ± 36 | 7.39 ± 0.22 | 6.28 ± 0.09 | 7.68 ± 0.10 | 1.39 ± 0.02 | 0.66 ± 0.01 | 0.73 ± 0.01 | 0.42 ± 0.01 |
| $K^- \pi^- \pi^+$ | 484 ± 76 | 23.61 ± 0.78 | 16.02 ± 0.17 | 18.61 ± 0.19 | 3.54 ± 0.03 | 1.63 ± 0.02 | 1.78 ± 0.02 | 1.20 ± 0.03 |
| $K_S^0 K_S^0 \pi^-$ | 122 ± 19 | 10.12 ± 0.32 | 7.16 ± 0.14 | 8.62 ± 0.16 | 1.69 ± 0.03 | 0.80 ± 0.02 | 0.81 ± 0.02 | 0.54 ± 0.02 |
| $K_S^0 K^+ \pi^- \pi^-$ | 370 ± 37 | 8.77 ± 0.17 | 6.77 ± 0.12 | 7.48 ± 0.13 | 1.57 ± 0.02 | 0.73 ± 0.02 | 0.71 ± 0.01 | 0.40 ± 0.02 |
| $K_S^0 K^- \pi^+ \pi^-$ | 153 ± 28 | 8.94 ± 0.30 | 6.25 ± 0.06 | 6.80 ± 0.07 | 1.42 ± 0.01 | 0.66 ± 0.01 | 0.65 ± 0.01 | 0.37 ± 0.01 |
| $\eta_{\gamma\gamma} \pi^-$ | 476 ± 56 | 19.16 ± 0.47 | 15.96 ± 0.08 | 20.95 ± 0.09 | 3.52 ± 0.02 | 1.62 ± 0.01 | 2.00 ± 0.01 | 1.45 ± 0.01 |
| $\eta_{\pi^+ \pi^- \pi^0} \pi^-$ | 102 ± 20 | 10.81 ± 0.44 | 8.36 ± 0.06 | 10.48 ± 0.07 | 1.89 ± 0.01 | 0.88 ± 0.01 | 0.99 ± 0.01 | 0.63 ± 0.01 |
| $\eta'_{\pi^+ \pi^- \eta} \pi^-$ | 238 ± 25 | 11.13 ± 0.26 | 8.59 ± 0.06 | 11.13 ± 0.07 | 1.88 ± 0.01 | 0.89 ± 0.01 | 1.06 ± 0.01 | 0.68 ± 0.01 |
| $\eta'_{\gamma\rho} \pi^-$ | 462 ± 50 | 13.24 ± 0.34 | 10.89 ± 0.07 | 13.99 ± 0.08 | 2.46 ± 0.01 | 1.13 ± 0.01 | 1.33 ± 0.01 | 0.82 ± 0.01 |
| $\eta_{\gamma\gamma} \rho^-$ | 624 ± 93 | 7.86 ± 0.27 | 7.39 ± 0.06 | 10.30 ± 0.07 | 1.68 ± 0.01 | 0.77 ± 0.01 | 1.01 ± 0.01 | 0.68 ± 0.01 |

TABLE XIII. The single-tag yields (N_{ST}), single-tag efficiencies (ϵ_{ST}), and double-tag efficiencies for each tag mode at 4.310–4.315 GeV. The $\epsilon_{\text{DT}}^{\mu_a\nu}$ and $\epsilon_{\text{DT}}^{\mu_b\nu}$ correspond to the double-tag efficiencies for $D_s^+ \rightarrow \mu_a^+ \nu_\mu$ and $D_s^+ \rightarrow \mu_b^+ \nu_\mu$; the $\epsilon_{\text{DT}}^{\tau_e\nu}$, $\epsilon_{\text{DT}}^{\tau_\mu\nu}$, $\epsilon_{\text{DT}}^{\tau_\pi\nu}$, and $\epsilon_{\text{DT}}^{\tau_\rho\nu}$ correspond to the double-tag efficiencies for $D_s^+ \rightarrow \tau_e^+ \nu_\tau$, $D_s^+ \rightarrow \tau_\mu^+ \nu_\tau$, $D_s^+ \rightarrow \tau_\pi^+ \nu_\tau$, and $D_s^+ \rightarrow \tau_\rho^+ \nu_\tau$, respectively. The efficiencies include the BF of D_s^{*+} and τ^+ decays. The uncertainties are statistical only.

| D_s^- tag mode | N_{ST} | ϵ_{ST} (%) | $\epsilon_{\text{DT}}^{\mu_a\nu}$ (%) | $\epsilon_{\text{DT}}^{\mu_b\nu}$ (%) | $\epsilon_{\text{DT}}^{\tau_e\nu}$ (%) | $\epsilon_{\text{DT}}^{\tau_\mu\nu}$ (%) | $\epsilon_{\text{DT}}^{\tau_\pi\nu}$ (%) | $\epsilon_{\text{DT}}^{\tau_\rho\nu}$ (%) |
|----------------------------------|-----------------|----------------------------|---------------------------------------|---------------------------------------|--|--|--|---|
| $K^+ K^- \pi^-$ | 2014 ± 83 | 16.86 ± 0.14 | 12.60 ± 0.07 | 13.34 ± 0.08 | 2.80 ± 0.01 | 1.32 ± 0.01 | 1.26 ± 0.01 | 0.81 ± 0.01 |
| $K^+ K^- \pi^- \pi^0$ | 722 ± 94 | 5.70 ± 0.18 | 4.25 ± 0.06 | 4.17 ± 0.06 | 0.97 ± 0.01 | 0.46 ± 0.01 | 0.41 ± 0.01 | 0.21 ± 0.01 |
| $\pi^- \pi^+ \pi^-$ | 415 ± 98 | 22.94 ± 0.73 | 16.02 ± 0.08 | 19.66 ± 0.09 | 3.52 ± 0.02 | 1.62 ± 0.01 | 1.89 ± 0.01 | 1.36 ± 0.01 |
| $K_S^0 K^-$ | 443 ± 32 | 19.15 ± 0.28 | 14.22 ± 0.09 | 17.12 ± 0.10 | 3.15 ± 0.02 | 1.47 ± 0.01 | 1.60 ± 0.01 | 1.16 ± 0.01 |
| $K_S^0 K^- \pi^0$ | 188 ± 46 | 6.63 ± 0.42 | 5.51 ± 0.09 | 6.74 ± 0.10 | 1.23 ± 0.02 | 0.59 ± 0.01 | 0.64 ± 0.01 | 0.41 ± 0.01 |
| $K^- \pi^- \pi^+$ | 254 ± 48 | 27.59 ± 1.31 | 14.16 ± 0.16 | 16.87 ± 0.18 | 3.15 ± 0.03 | 1.45 ± 0.02 | 1.57 ± 0.02 | 1.12 ± 0.03 |
| $K_S^0 K_S^0 \pi^-$ | 85 ± 18 | 9.49 ± 0.52 | 6.49 ± 0.14 | 7.95 ± 0.15 | 1.51 ± 0.03 | 0.71 ± 0.02 | 0.81 ± 0.02 | 0.54 ± 0.02 |
| $K_S^0 K^+ \pi^- \pi^-$ | 237 ± 42 | 8.31 ± 0.27 | 6.31 ± 0.11 | 7.29 ± 0.12 | 1.46 ± 0.02 | 0.70 ± 0.02 | 0.68 ± 0.01 | 0.38 ± 0.02 |
| $K_S^0 K^- \pi^+ \pi^-$ | 156 ± 45 | 9.28 ± 0.58 | 5.86 ± 0.06 | 6.47 ± 0.07 | 1.29 ± 0.01 | 0.59 ± 0.01 | 0.60 ± 0.01 | 0.36 ± 0.01 |
| $\eta_{\gamma\gamma} \pi^-$ | 211 ± 55 | 15.60 ± 0.71 | 13.77 ± 0.08 | 18.24 ± 0.09 | 3.03 ± 0.01 | 1.38 ± 0.01 | 1.74 ± 0.01 | 1.32 ± 0.01 |
| $\eta_{\pi^+ \pi^- \pi^0} \pi^-$ | 70 ± 17 | 8.87 ± 0.62 | 7.33 ± 0.06 | 9.40 ± 0.07 | 1.63 ± 0.01 | 0.77 ± 0.01 | 0.87 ± 0.01 | 0.56 ± 0.01 |
| $\eta'_{\pi^+ \pi^- \eta} \pi^-$ | 139 ± 21 | 9.21 ± 0.36 | 7.37 ± 0.06 | 9.78 ± 0.07 | 1.66 ± 0.01 | 0.78 ± 0.01 | 0.92 ± 0.01 | 0.64 ± 0.01 |
| $\eta'_{\gamma\rho} \pi^-$ | 269 ± 55 | 12.80 ± 0.55 | 9.65 ± 0.06 | 12.31 ± 0.07 | 2.17 ± 0.01 | 1.01 ± 0.01 | 1.18 ± 0.01 | 0.76 ± 0.01 |
| $\eta_{\gamma\gamma} \rho^-$ | 555 ± 102 | 6.23 ± 0.37 | 6.38 ± 0.05 | 8.94 ± 0.06 | 1.42 ± 0.01 | 0.67 ± 0.01 | 0.86 ± 0.01 | 0.59 ± 0.01 |

TABLE XIV. The single-tag yields (N_{ST}), single-tag efficiencies (ϵ_{ST}), and double-tag efficiencies for each tag mode at 4.400 GeV. The $\epsilon_{\text{DT}}^{\mu_a\nu}$ and $\epsilon_{\text{DT}}^{\mu_b\nu}$ correspond to the double-tag efficiencies for $D_s^+ \rightarrow \mu_a^+ \nu_\mu$ and $D_s^+ \rightarrow \mu_b^+ \nu_\mu$; the $\epsilon_{\text{DT}}^{\tau_e\nu}$, $\epsilon_{\text{DT}}^{\tau_\mu\nu}$, $\epsilon_{\text{DT}}^{\tau_\pi\nu}$, and $\epsilon_{\text{DT}}^{\tau_\rho\nu}$ correspond to the double-tag efficiencies for $D_s^+ \rightarrow \tau_e^+ \nu_\tau$, $D_s^+ \rightarrow \tau_\mu^+ \nu_\tau$, $D_s^+ \rightarrow \tau_\pi^+ \nu_\tau$, and $D_s^+ \rightarrow \tau_\rho^+ \nu_\tau$, respectively. The efficiencies include the BF of D_s^{*+} and τ^+ decays. The uncertainties are statistical only.

| D_s^- tag mode | N_{ST} | ϵ_{ST} (%) | $\epsilon_{\text{DT}}^{\mu_a\nu}$ (%) | $\epsilon_{\text{DT}}^{\mu_b\nu}$ (%) | $\epsilon_{\text{DT}}^{\tau_e\nu}$ (%) | $\epsilon_{\text{DT}}^{\tau_\mu\nu}$ (%) | $\epsilon_{\text{DT}}^{\tau_\pi\nu}$ (%) | $\epsilon_{\text{DT}}^{\tau_\rho\nu}$ (%) |
|------------------|-----------------|----------------------------|---------------------------------------|---------------------------------------|--|--|--|---|
| $K^+ K^- \pi^-$ | 1544 ± 83 | 17.06 ± 0.19 | 12.68 ± 0.07 | 13.80 ± 0.08 | 2.83 ± 0.01 | 1.29 ± 0.01 | 1.26 ± 0.01 | 0.87 ± 0.01 |
| $K_S^0 K^-$ | 311 ± 27 | 20.05 ± 0.36 | 14.18 ± 0.09 | 17.15 ± 0.10 | 3.12 ± 0.02 | 1.43 ± 0.01 | 1.60 ± 0.01 | 1.24 ± 0.02 |

TABLE XV. The single-tag yields (N_{ST}), single-tag efficiencies (ϵ_{ST}), and double-tag efficiencies for each tag mode at 4.420 GeV. The $\epsilon_{\text{DT}}^{\mu_a\nu}$ and $\epsilon_{\text{DT}}^{\mu_b\nu}$ correspond to the double-tag efficiencies for $D_s^+ \rightarrow \mu_a^+ \nu_\mu$ and $D_s^+ \rightarrow \mu_b^+ \nu_\mu$; the $\epsilon_{\text{DT}}^{\tau_e\nu}$, $\epsilon_{\text{DT}}^{\tau_\mu\nu}$, $\epsilon_{\text{DT}}^{\tau_\pi\nu}$, and $\epsilon_{\text{DT}}^{\tau_\rho\nu}$ correspond to the double-tag efficiencies for $D_s^+ \rightarrow \tau_e^+ \nu_\tau$, $D_s^+ \rightarrow \tau_\mu^+ \nu_\tau$, $D_s^+ \rightarrow \tau_\pi^+ \nu_\tau$, and $D_s^+ \rightarrow \tau_\rho^+ \nu_\tau$, respectively. The efficiencies include the BF of D_s^{*+} and τ^+ decays. The uncertainties are statistical only.

| D_s^- tag mode | N_{ST} | ϵ_{ST} (%) | $\epsilon_{\text{DT}}^{\mu_a\nu}$ (%) | $\epsilon_{\text{DT}}^{\mu_b\nu}$ (%) | $\epsilon_{\text{DT}}^{\tau_e\nu}$ (%) | $\epsilon_{\text{DT}}^{\tau_\mu\nu}$ (%) | $\epsilon_{\text{DT}}^{\tau_\pi\nu}$ (%) | $\epsilon_{\text{DT}}^{\tau_\rho\nu}$ (%) |
|----------------------------------|-----------------|----------------------------|---------------------------------------|---------------------------------------|--|--|--|---|
| $K^+ K^- \pi^-$ | 5297 ± 138 | 18.44 ± 0.10 | 13.67 ± 0.08 | 15.07 ± 0.08 | 3.08 ± 0.02 | 1.42 ± 0.01 | 1.39 ± 0.01 | 1.00 ± 0.01 |
| $K^+ K^- \pi^- \pi^0$ | 1539 ± 218 | 5.36 ± 0.11 | 4.96 ± 0.06 | 5.18 ± 0.06 | 1.10 ± 0.01 | 0.51 ± 0.01 | 0.49 ± 0.01 | 0.31 ± 0.01 |
| $\pi^- \pi^+ \pi^-$ | 1185 ± 135 | 22.40 ± 0.50 | 17.46 ± 0.08 | 21.69 ± 0.09 | 3.84 ± 0.02 | 1.76 ± 0.01 | 2.02 ± 0.01 | 1.58 ± 0.01 |
| $K_S^0 K^-$ | 1195 ± 53 | 21.90 ± 0.19 | 15.85 ± 0.10 | 19.25 ± 0.11 | 3.47 ± 0.02 | 1.59 ± 0.01 | 1.80 ± 0.01 | 1.41 ± 0.02 |
| $K_S^0 K^- \pi^0$ | 485 ± 84 | 7.81 ± 0.30 | 6.09 ± 0.09 | 7.62 ± 0.10 | 1.37 ± 0.02 | 0.64 ± 0.01 | 0.71 ± 0.01 | 0.49 ± 0.01 |
| $K^- \pi^- \pi^+$ | 684 ± 135 | 21.28 ± 0.90 | 15.63 ± 0.17 | 18.90 ± 0.19 | 3.43 ± 0.03 | 1.55 ± 0.02 | 1.76 ± 0.02 | 1.33 ± 0.03 |
| $K_S^0 K_S^0 \pi^-$ | 192 ± 35 | 10.32 ± 0.34 | 8.02 ± 0.15 | 9.76 ± 0.17 | 1.75 ± 0.03 | 0.84 ± 0.02 | 0.88 ± 0.02 | 0.64 ± 0.02 |
| $K_S^0 K^+ \pi^- \pi^-$ | 588 ± 58 | 9.58 ± 0.19 | 7.51 ± 0.12 | 8.56 ± 0.13 | 1.68 ± 0.02 | 0.78 ± 0.02 | 0.80 ± 0.01 | 0.52 ± 0.02 |
| $K_S^0 K^- \pi^+ \pi^-$ | 314 ± 71 | 10.05 ± 0.37 | 6.77 ± 0.07 | 7.73 ± 0.07 | 1.50 ± 0.01 | 0.69 ± 0.01 | 0.70 ± 0.01 | 0.46 ± 0.01 |
| $\eta_{\gamma\gamma} \pi^-$ | 591 ± 79 | 18.65 ± 0.49 | 14.32 ± 0.08 | 19.12 ± 0.09 | 3.13 ± 0.01 | 1.42 ± 0.01 | 1.78 ± 0.01 | 1.44 ± 0.01 |
| $\eta_{\pi^+ \pi^- \pi^0} \pi^-$ | 164 ± 29 | 9.82 ± 0.44 | 7.61 ± 0.06 | 9.88 ± 0.07 | 1.69 ± 0.01 | 0.79 ± 0.01 | 0.93 ± 0.01 | 0.66 ± 0.01 |
| $\eta'_{\pi^+ \pi^- \eta} \pi^-$ | 389 ± 30 | 10.13 ± 0.25 | 8.03 ± 0.07 | 10.64 ± 0.08 | 1.77 ± 0.01 | 0.82 ± 0.01 | 0.98 ± 0.01 | 0.72 ± 0.01 |
| $\eta'_{\gamma\rho} \pi^-$ | 949 ± 120 | 13.41 ± 0.36 | 10.44 ± 0.07 | 13.49 ± 0.08 | 2.32 ± 0.01 | 1.07 ± 0.01 | 1.26 ± 0.01 | 0.89 ± 0.01 |
| $\eta_{\gamma\gamma} \rho^-$ | 1318 ± 227 | 7.58 ± 0.26 | 6.32 ± 0.05 | 8.87 ± 0.06 | 1.40 ± 0.01 | 0.65 ± 0.01 | 0.84 ± 0.01 | 0.61 ± 0.01 |

TABLE XVI. The single-tag yields (N_{ST}), single-tag efficiencies (ϵ_{ST}), and double-tag efficiencies for each tag mode at 4.440 GeV. The $\epsilon_{\text{DT}}^{\mu_a\nu}$ and $\epsilon_{\text{DT}}^{\mu_b\nu}$ correspond to the double-tag efficiencies for $D_s^+ \rightarrow \mu_a^+ \nu_\mu$ and $D_s^+ \rightarrow \mu_b^+ \nu_\mu$; the $\epsilon_{\text{DT}}^{\tau_a\nu}$, $\epsilon_{\text{DT}}^{\tau_b\nu}$, $\epsilon_{\text{DT}}^{\tau_c\nu}$, and $\epsilon_{\text{DT}}^{\tau_d\nu}$ correspond to the double-tag efficiencies for $D_s^+ \rightarrow \tau_e^+ \nu_\tau$, $D_s^+ \rightarrow \tau_\mu^+ \nu_\tau$, $D_s^+ \rightarrow \tau_\pi^+ \nu_\tau$, and $D_s^+ \rightarrow \tau_\rho^+ \nu_\tau$, respectively. The efficiencies include the BFs of D_s^{*+} and τ^+ decays. The uncertainties are statistical only.

| D_s^- tag mode | N_{ST} | ϵ_{ST} (%) | $\epsilon_{\text{DT}}^{\mu_a\nu}$ (%) | $\epsilon_{\text{DT}}^{\mu_b\nu}$ (%) | $\epsilon_{\text{DT}}^{\tau_a\nu}$ (%) | $\epsilon_{\text{DT}}^{\tau_b\nu}$ (%) | $\epsilon_{\text{DT}}^{\tau_c\nu}$ (%) | $\epsilon_{\text{DT}}^{\tau_d\nu}$ (%) |
|----------------------------------|-----------------|----------------------------|---------------------------------------|---------------------------------------|--|--|--|--|
| $K^+ K^- \pi^-$ | 3512 ± 100 | 17.87 ± 0.11 | 13.45 ± 0.08 | 15.05 ± 0.08 | 3.01 ± 0.01 | 1.37 ± 0.01 | 1.38 ± 0.01 | 0.95 ± 0.01 |
| $K^+ K^- \pi^- \pi^0$ | 1341 ± 158 | 5.04 ± 0.11 | 4.86 ± 0.06 | 5.19 ± 0.06 | 1.09 ± 0.01 | 0.50 ± 0.01 | 0.46 ± 0.01 | 0.28 ± 0.01 |
| $\pi^- \pi^+ \pi^-$ | 618 ± 90 | 24.03 ± 0.55 | 17.07 ± 0.08 | 21.38 ± 0.09 | 3.82 ± 0.02 | 1.73 ± 0.01 | 2.01 ± 0.01 | 1.56 ± 0.01 |
| $K_S^0 K^-$ | 769 ± 41 | 21.09 ± 0.23 | 15.50 ± 0.09 | 19.01 ± 0.11 | 3.35 ± 0.02 | 1.52 ± 0.01 | 1.73 ± 0.01 | 1.32 ± 0.02 |
| $K_S^0 K^- \pi^0$ | 244 ± 67 | 6.79 ± 0.32 | 5.87 ± 0.09 | 7.36 ± 0.10 | 1.30 ± 0.02 | 0.60 ± 0.01 | 0.69 ± 0.01 | 0.46 ± 0.01 |
| $K^- \pi^- \pi^+$ | 522 ± 131 | 21.68 ± 1.03 | 15.07 ± 0.17 | 18.40 ± 0.19 | 3.42 ± 0.03 | 1.56 ± 0.02 | 1.68 ± 0.02 | 1.30 ± 0.03 |
| $K_S^0 K_S^0 \pi^-$ | 156 ± 26 | 9.64 ± 0.38 | 7.34 ± 0.14 | 9.08 ± 0.16 | 1.66 ± 0.03 | 0.72 ± 0.02 | 0.83 ± 0.02 | 0.55 ± 0.02 |
| $K_S^0 K^+ \pi^- \pi^-$ | 362 ± 38 | 9.15 ± 0.20 | 7.08 ± 0.12 | 8.00 ± 0.13 | 1.54 ± 0.02 | 0.72 ± 0.02 | 0.73 ± 0.01 | 0.49 ± 0.02 |
| $K_S^0 K^- \pi^+ \pi^-$ | 216 ± 37 | 8.22 ± 0.38 | 6.28 ± 0.06 | 7.20 ± 0.07 | 1.43 ± 0.01 | 0.64 ± 0.01 | 0.66 ± 0.01 | 0.42 ± 0.01 |
| $\eta_{\gamma\gamma} \pi^-$ | 332 ± 76 | 16.88 ± 0.85 | 13.94 ± 0.08 | 18.81 ± 0.09 | 3.10 ± 0.01 | 1.39 ± 0.01 | 1.75 ± 0.01 | 1.43 ± 0.02 |
| $\eta_{\pi^+ \pi^- \pi^0} \pi^-$ | 134 ± 23 | 9.52 ± 0.50 | 7.49 ± 0.06 | 9.84 ± 0.07 | 1.65 ± 0.01 | 0.75 ± 0.01 | 0.90 ± 0.01 | 0.64 ± 0.01 |
| $\eta'_{\pi^+ \pi^- \eta} \pi^-$ | 213 ± 21 | 9.83 ± 0.30 | 7.87 ± 0.06 | 10.50 ± 0.07 | 1.73 ± 0.01 | 0.77 ± 0.01 | 0.96 ± 0.01 | 0.72 ± 0.01 |
| $\eta'_{\gamma\rho} \pi^-$ | 608 ± 68 | 12.63 ± 0.44 | 10.25 ± 0.07 | 13.36 ± 0.08 | 2.28 ± 0.01 | 1.05 ± 0.01 | 1.24 ± 0.01 | 0.87 ± 0.01 |
| $\eta_{\gamma\gamma} \rho^-$ | 672 ± 129 | 6.09 ± 0.36 | 6.16 ± 0.05 | 8.70 ± 0.06 | 1.38 ± 0.01 | 0.63 ± 0.01 | 0.82 ± 0.01 | 0.61 ± 0.01 |

TABLE XVII. The single-tag yields (N_{ST}), single-tag efficiencies (ϵ_{ST}), and double-tag efficiencies for each tag mode at 4.470–4.699 GeV. The $\epsilon_{\text{DT}}^{\mu_a\nu}$ and $\epsilon_{\text{DT}}^{\mu_b\nu}$ correspond to the double-tag efficiencies for $D_s^+ \rightarrow \mu_a^+ \nu_\mu$ and $D_s^+ \rightarrow \mu_b^+ \nu_\mu$; the $\epsilon_{\text{DT}}^{\tau_a\nu}$, $\epsilon_{\text{DT}}^{\tau_b\nu}$, $\epsilon_{\text{DT}}^{\tau_c\nu}$, and $\epsilon_{\text{DT}}^{\tau_d\nu}$ correspond to the double-tag efficiencies for $D_s^+ \rightarrow \tau_e^+ \nu_\tau$, $D_s^+ \rightarrow \tau_\mu^+ \nu_\tau$, $D_s^+ \rightarrow \tau_\pi^+ \nu_\tau$, and $D_s^+ \rightarrow \tau_\rho^+ \nu_\tau$, respectively. The efficiencies include the BFs of D_s^{*+} and τ^+ decays. The uncertainties are statistical only.

| D_s^- tag mode | N_{ST} | ϵ_{ST} (%) | $\epsilon_{\text{DT}}^{\mu_a\nu}$ (%) | $\epsilon_{\text{DT}}^{\mu_b\nu}$ (%) | $\epsilon_{\text{DT}}^{\tau_a\nu}$ (%) | $\epsilon_{\text{DT}}^{\tau_b\nu}$ (%) | $\epsilon_{\text{DT}}^{\tau_c\nu}$ (%) | $\epsilon_{\text{DT}}^{\tau_d\nu}$ (%) |
|----------------------------------|-----------------|----------------------------|---------------------------------------|---------------------------------------|--|--|--|--|
| $K^+ K^- \pi^-$ | 10840 ± 266 | 15.44 ± 0.07 | 11.12 ± 0.03 | 12.85 ± 0.03 | 2.57 ± 0.01 | 1.14 ± 0.01 | 1.12 ± 0.01 | 0.84 ± 0.01 |
| $K^+ K^- \pi^- \pi^0$ | 4412 ± 487 | 4.99 ± 0.11 | 4.24 ± 0.02 | 4.77 ± 0.03 | 0.98 ± 0.01 | 0.44 ± 0.01 | 0.41 ± 0.01 | 0.26 ± 0.01 |
| $\pi^- \pi^+ \pi^-$ | 2870 ± 383 | 19.22 ± 0.45 | 13.73 ± 0.03 | 17.63 ± 0.04 | 3.16 ± 0.01 | 1.38 ± 0.01 | 1.56 ± 0.01 | 1.25 ± 0.01 |
| $K_S^0 K^-$ | 2217 ± 91 | 17.41 ± 0.15 | 12.33 ± 0.04 | 15.44 ± 0.04 | 2.82 ± 0.01 | 1.22 ± 0.01 | 1.35 ± 0.01 | 1.10 ± 0.01 |
| $K_S^0 K^- \pi^0$ | 643 ± 158 | 5.56 ± 0.24 | 4.91 ± 0.04 | 6.22 ± 0.04 | 1.12 ± 0.01 | 0.50 ± 0.01 | 0.55 ± 0.01 | 0.40 ± 0.01 |
| $K_S^0 K_S^0 \pi^-$ | 346 ± 68 | 7.77 ± 0.26 | 6.08 ± 0.06 | 7.72 ± 0.07 | 1.39 ± 0.01 | 0.63 ± 0.01 | 0.68 ± 0.01 | 0.47 ± 0.01 |
| $K_S^0 K^+ \pi^- \pi^-$ | 1114 ± 97 | 8.01 ± 0.14 | 6.03 ± 0.05 | 7.07 ± 0.05 | 1.38 ± 0.01 | 0.60 ± 0.01 | 0.60 ± 0.01 | 0.42 ± 0.01 |
| $K_S^0 K^- \pi^+ \pi^-$ | 376 ± 90 | 8.10 ± 0.30 | 5.38 ± 0.03 | 6.33 ± 0.03 | 1.24 ± 0.01 | 0.55 ± 0.01 | 0.54 ± 0.01 | 0.37 ± 0.01 |
| $\eta'_{\pi^+ \pi^- \eta} \pi^-$ | 735 ± 87 | 8.17 ± 0.22 | 6.30 ± 0.02 | 8.62 ± 0.03 | 1.44 ± 0.00 | 0.64 ± 0.01 | 0.76 ± 0.01 | 0.60 ± 0.01 |
| $\eta'_{\gamma\rho} \pi^-$ | 1603 ± 252 | 10.26 ± 0.30 | 8.16 ± 0.03 | 10.91 ± 0.03 | 1.90 ± 0.01 | 0.83 ± 0.01 | 0.96 ± 0.01 | 0.72 ± 0.01 |

[1] D. Silverman and H. Yao, *Phys. Rev. D* **38**, 214 (1988).
[2] S. Navas *et al.* (Particle Data Group), *Phys. Rev. D* **110**, 030001 (2024).
[3] A. Bazavov *et al.* (Fermilab Lattice and MILC Collaborations), *Phys. Rev. D* **98**, 074512 (2018).
[4] A. Bazavov *et al.* (Fermilab Lattice and MILC Collaborations), *Phys. Rev. D* **90**, 074509 (2014).
[5] N. Carrasco *et al.*, *Phys. Rev. D* **91**, 054507 (2014).

[6] P. A. Boyle, L. Del Debbio, A. Jüttner, A. Khamseh, F. Sanfilippo, and J. T. Tsang, *J. High Energy Phys.* **12** (2017) 008.
[7] A. Bazavov *et al.* (Fermilab Lattice and MILC Collaborations), *Phys. Rev. D* **85**, 114506 (2012).
[8] C. T. H. Davies, C. McNeile, E. Follana, G. P. Lepage, H. Na, and J. Shigemitsu, *Phys. Rev. D* **82**, 114504 (2010).
[9] P. U. E. Onyisi *et al.* (CLEO Collaboration), *Phys. Rev. D* **79**, 052002 (2009).

- [10] P. Naik *et al.* (CLEO Collaboration), *Phys. Rev. D* **80**, 112004 (2009).
- [11] J. P. Alexander *et al.* (CLEO Collaboration), *Phys. Rev. D* **79**, 052001 (2009).
- [12] del Amo Sanchez *et al.* (BABAR Collaboration), *Phys. Rev. D* **82**, 091103 (2010).
- [13] A. Zupanc *et al.* (Belle Collaboration), *J. High Energy Phys.* **09** (2013) 139.
- [14] M. Ablikim *et al.* (BESIII Collaboration), *Phys. Rev. D* **94**, 072004 (2016).
- [15] M. Ablikim *et al.* (BESIII Collaboration), *Phys. Rev. Lett.* **122**, 071802 (2019).
- [16] M. Ablikim *et al.* (BESIII Collaboration), *Phys. Rev. D* **104**, 032001 (2021).
- [17] M. Ablikim *et al.* (BESIII Collaboration), *Phys. Rev. D* **104**, 052009 (2021).
- [18] M. Ablikim *et al.* (BESIII Collaboration), *Phys. Rev. Lett.* **127**, 171801 (2021).
- [19] M. Ablikim *et al.* (BESIII Collaboration), *Phys. Rev. D* **108**, 092014 (2023).
- [20] M. Ablikim *et al.* (BESIII Collaboration), *J. High Energy Phys.* **09** (2023) 124.
- [21] M. Ablikim *et al.* (BESIII Collaboration), *Phys. Rev. D* **108**, 112001 (2023).
- [22] B. C. Ke, J. Koponen, H. B. Li, and Y. Zheng, *Annu. Rev. Nucl. Part. Sci.* **73**, 285 (2023).
- [23] H. B. Li and X. R. Lyu, *Natl. Sci. Rev.* **8**, nwab181 (2021).
- [24] M. Ablikim *et al.* (BESIII Collaboration), *Nucl. Instrum. Methods Phys. Res., Sect. A* **614**, 345 (2010).
- [25] C. H. Yu *et al.*, *Proceedings of IPAC2016, Busan, Korea* (2016), 10.18429/JACoW-IPAC2016-TUYA01.
- [26] X. Li *et al.*, *Radiat. Detect. Technol. Methods* **1**, 13 (2017).
- [27] Y. Guo *et al.*, *Radiat. Detect. Technol. Methods* **1**, 14 (2017).
- [28] S. Agostinelli *et al.* (GEANT4 Collaboration), *Nucl. Instrum. Methods Phys. Res., Sect. A* **506**, 250 (2003).
- [29] S. Jadach, B. F. L. Ward, and Z. Was, *Comput. Phys. Commun.* **130**, 260 (2000); *Phys. Rev. D* **63**, 113009 (2001).
- [30] R. G. Ping, *Chin. Phys. C* **38**, 083001 (2014).
- [31] D. J. Lange, *Nucl. Instrum. Methods Phys. Res., Sect. A* **462**, 152 (2001); R. G. Ping, *Chin. Phys. C* **32**, 599 (2008).
- [32] J. C. Chen, G. S. Huang, X. R. Qi, D. H. Zhang, and Y. S. Zhu, *Phys. Rev. D* **62**, 034003 (2000).
- [33] E. Richter-Was, *Phys. Lett. B* **303**, 163 (1993).
- [34] M. Ablikim *et al.* (BESIII Collaboration), *Phys. Rev. Lett.* **131**, 151903 (2023).
- [35] M. Ablikim *et al.* (BESIII Collaboration), *Phys. Rev. Lett.* **132**, 091802 (2024).
- [36] M. Ablikim *et al.* (BESIII Collaboration), *Phys. Rev. D* **108**, 092003 (2023).
- [37] H. Albrecht *et al.* (ARGUS Collaboration), *Phys. Lett. B* **241**, 278 (1990).
- [38] M. Ablikim *et al.* (BESIII Collaboration), *Phys. Rev. D* **83**, 112005 (2011).
- [39] M. Ablikim *et al.* (BESIII Collaboration), *Phys. Rev. D* **99**, 031101 (2019).
- [40] M. Ablikim *et al.* (BESIII Collaboration), Measurement of the cross section for $e^+e^- \rightarrow D_s^+D_s^-$ up to 4.7 GeV (to be published).
- [41] M. Schmelling, *Phys. Scr.* **51**, 676 (1995).

M. Ablikim,¹ M. N. Achasov,^{4,c} P. Adlarson,⁷⁵ O. Afedulidis,³ X. C. Ai,⁸⁰ R. Aliberti,³⁵ A. Amoroso,^{74a,74c} Q. An,^{71,58,a} Y. Bai,⁵⁷ O. Bakina,³⁶ I. Balossino,^{29a} Y. Ban,^{46,h} H.-R. Bao,⁶³ V. Batozskaya,^{1,44} K. Begzsuren,³² N. Berger,³⁵ M. Berlowski,⁴⁴ M. Bertani,^{28a} D. Bettoni,^{29a} F. Bianchi,^{74a,74c} E. Bianco,^{74a,74c} A. Bortone,^{74a,74c} I. Boyko,³⁶ R. A. Briere,⁵ A. Brueggemann,⁶⁸ H. Cai,⁷⁶ X. Cai,^{1,58} A. Calcaterra,^{28a} G. F. Cao,^{1,63} N. Cao,^{1,63} S. A. Cetin,^{62a} J. F. Chang,^{1,58} G. R. Che,⁴³ G. Chelkov,^{36,b} C. Chen,⁴³ C. H. Chen,⁹ Chao Chen,⁵⁵ G. Chen,¹ H. S. Chen,^{1,63} H. Y. Chen,²⁰ M. L. Chen,^{1,58,63} S. J. Chen,⁴² S. L. Chen,⁴⁵ S. M. Chen,⁶¹ T. Chen,^{1,63} X. R. Chen,^{31,63} X. T. Chen,^{1,63} Y. B. Chen,^{1,58} Y. Q. Chen,³⁴ Z. J. Chen,^{25,i} Z. Y. Chen,^{1,63} S. K. Choi,¹⁰ G. Cibinetto,^{29a} F. Cossio,^{74c} J. J. Cui,⁵⁰ H. L. Dai,^{1,58} J. P. Dai,⁷⁸ A. Dbeyssi,¹⁸ R. E. de Boer,³ D. Dedovich,³⁶ C. Q. Deng,⁷² Z. Y. Deng,¹ A. Denig,³⁵ I. Denysenko,³⁶ M. Destefanis,^{74a,74c} F. De Mori,^{74a,74c} B. Ding,^{66,1} X. X. Ding,^{46,h} Y. Ding,³⁴ Y. Ding,⁴⁰ J. Dong,^{1,58} L. Y. Dong,^{1,63} M. Y. Dong,^{1,58,63} X. Dong,⁷⁶ M. C. Du,¹ S. X. Du,⁸⁰ Y. Y. Duan,⁵⁵ Z. H. Duan,⁴² P. Egorov,^{36,b} Y. H. Fan,⁴⁵ J. Fang,⁵⁹ J. Fang,^{1,58} S. S. Fang,^{1,63} W. X. Fang,¹ Y. Fang,¹ Y. Q. Fang,^{1,58} R. Farinelli,^{29a} L. Fava,^{74b,74c} F. Feldbauer,³ G. Felici,^{28a} C. Q. Feng,^{71,58} J. H. Feng,⁵⁹ Y. T. Feng,^{71,58} M. Fritsch,³ C. D. Fu,¹ J. L. Fu,⁶³ Y. W. Fu,^{1,63} H. Gao,⁶³ X. B. Gao,⁴¹ Y. N. Gao,^{46,h} Yang Gao,^{71,58} S. Garbolino,^{74c} I. Garzia,^{29a,29b} L. Ge,⁸⁰ P. T. Ge,⁷⁶ Z. W. Ge,⁴² C. Geng,⁵⁹ E. M. Gersabeck,⁶⁷ A. Gilman,⁶⁹ K. Goetzen,¹³ L. Gong,⁴⁰ W. X. Gong,^{1,58} W. Gradl,³⁵ S. Gramigna,^{29a,29b} M. Greco,^{74a,74c} M. H. Gu,^{1,58} Y. T. Gu,¹⁵ C. Y. Guan,^{1,63} A. Q. Guo,^{31,63} L. B. Guo,⁴¹ M. J. Guo,⁵⁰ R. P. Guo,⁴⁹ Y. P. Guo,^{12,g} A. Guskov,^{36,b} J. Gutierrez,²⁷ K. L. Han,⁶³ T. T. Han,¹ F. Hanisch,³ X. Q. Hao,¹⁹ F. A. Harris,⁶⁵ K. K. He,⁵⁵ K. L. He,^{1,63} F. H. Heinsius,³ C. H. Heinz,³⁵ Y. K. Heng,^{1,58,63} C. Herold,⁶⁰ T. Holtmann,³ P. C. Hong,³⁴ G. Y. Hou,^{1,63} X. T. Hou,^{1,63} Y. R. Hou,⁶³ Z. L. Hou,¹ B. Y. Hu,⁵⁹ H. M. Hu,^{1,63} J. F. Hu,^{56,j} S. L. Hu,^{12,g} T. Hu,^{1,58,63} Y. Hu,¹ G. S. Huang,^{71,58} K. X. Huang,⁵⁹ L. Q. Huang,^{31,63} X. T. Huang,⁵⁰ Y. P. Huang,¹ Y. S. Huang,⁵⁹ T. Hussain,⁷³ F. Hölzken,³ N. Hüskens,³⁵ N. in der Wiesche,⁶⁸ J. Jackson,²⁷ S. Janchiv,³² J. H. Jeong,¹⁰ Q. Ji,¹ Q. P. Ji,¹⁹ W. Ji,^{1,63} X. B. Ji,^{1,63} X. L. Ji,^{1,58} Y. Y. Ji,⁵⁰ X. Q. Jia,⁵⁰ Z. K. Jia,^{71,58} D. Jiang,^{1,63} H. B. Jiang,⁷⁶ P. C. Jiang,^{46,h}

S. S. Jiang,³⁹ T. J. Jiang,¹⁶ X. S. Jiang,^{1,58,63} Y. Jiang,⁶³ J. B. Jiao,⁵⁰ J. K. Jiao,³⁴ Z. Jiao,²³ S. Jin,⁴² Y. Jin,⁶⁶ M. Q. Jing,^{1,63}
 X. M. Jing,⁶³ T. Johansson,⁷⁵ S. Kabana,³³ N. Kalantar-Nayestanaki,⁶⁴ X. L. Kang,⁹ X. S. Kang,⁴⁰ M. Kavatsyuk,⁶⁴
 B. C. Ke,⁸⁰ V. Khachatryan,²⁷ A. Khoukaz,⁶⁸ R. Kiuchi,¹ O. B. Kolcu,^{62a} B. Kopf,³ M. Kuessner,³ X. Kui,^{1,63} N. Kumar,²⁶
 A. Kupsc,^{44,75} W. Kühn,³⁷ J. J. Lane,⁶⁷ L. Lavezzi,^{74a,74c} T. T. Lei,^{71,58} Z. H. Lei,^{71,58} M. Lellmann,³⁵ T. Lenz,³⁵ C. Li,⁴⁷
 C. Li,⁴³ C. H. Li,³⁹ Cheng Li,^{71,58} D. M. Li,⁸⁰ F. Li,^{1,58} G. Li,¹ H. B. Li,^{1,63} H. J. Li,¹⁹ H. N. Li,^{56j} Hui Li,⁴³ J. R. Li,⁶¹
 J. S. Li,⁵⁹ K. Li,¹ L. J. Li,^{1,63} L. K. Li,¹ Lei Li,⁴⁸ M. H. Li,⁴³ P. R. Li,^{38,k,l} Q. M. Li,^{1,63} Q. X. Li,⁵⁰ R. Li,^{17,31} S. X. Li,¹² T. Li,⁵⁰
 W. D. Li,^{1,63} W. G. Li,^{1,a} X. Li,^{1,63} X. H. Li,^{71,58} X. L. Li,⁵⁰ X. Y. Li,^{1,63} X. Z. Li,⁵⁹ Y. G. Li,^{46,h} Z. J. Li,⁵⁹ Z. Y. Li,⁷⁸
 C. Liang,⁴² H. Liang,^{1,63} H. Liang,^{71,58} Y. F. Liang,⁵⁴ Y. T. Liang,^{31,63} G. R. Liao,¹⁴ Y. P. Liao,^{1,63} J. Libby,²⁶ A. Limphirat,⁶⁰
 C. C. Lin,⁵⁵ D. X. Lin,^{31,63} T. Lin,¹ B. J. Liu,¹ B. X. Liu,⁷⁶ C. Liu,³⁴ C. X. Liu,¹ F. Liu,¹ F. H. Liu,⁵³ Feng Liu,⁶ G. M. Liu,^{56j}
 H. Liu,^{38,k,l} H. B. Liu,¹⁵ H. H. Liu,¹ H. M. Liu,^{1,63} Huihui Liu,²¹ J. B. Liu,^{71,58} J. Y. Liu,^{1,63} K. Liu,^{38,k,l} K. Y. Liu,⁴⁰ Ke Liu,²²
 L. Liu,^{71,58} L. C. Liu,⁴³ Lu Liu,⁴³ M. H. Liu,^{12,g} P. L. Liu,¹ Q. Liu,⁶³ S. B. Liu,^{71,58} T. Liu,^{12,g} W. K. Liu,⁴³ W. M. Liu,^{71,58}
 X. Liu,^{38,k,l} X. Liu,³⁹ Y. Liu,⁸⁰ Y. Liu,^{38,k,l} Y. B. Liu,⁴³ Z. A. Liu,^{1,58,63} Z. D. Liu,⁹ Z. Q. Liu,⁵⁰ X. C. Lou,^{1,58,63} F. X. Lu,⁵⁹
 H. J. Lu,²³ J. G. Lu,^{1,58} X. L. Lu,¹ Y. Lu,⁷ Y. P. Lu,^{1,58} Z. H. Lu,^{1,63} C. L. Luo,⁴¹ J. R. Luo,⁵⁹ M. X. Luo,⁷⁹ T. Luo,^{12,g}
 X. L. Luo,^{1,58} X. R. Lyu,⁶³ Y. F. Lyu,⁴³ F. C. Ma,⁴⁰ H. Ma,⁷⁸ H. L. Ma,¹ J. L. Ma,^{1,63} L. L. Ma,⁵⁰ M. M. Ma,^{1,63} Q. M. Ma,¹
 R. Q. Ma,^{1,63} T. Ma,^{71,58} X. T. Ma,^{1,63} X. Y. Ma,^{1,58} Y. Ma,^{46,h} Y. M. Ma,³¹ F. E. Maas,¹⁸ M. Maggiora,^{74a,74c} S. Malde,⁶⁹
 Y. J. Mao,^{46,h} Z. P. Mao,¹ S. Marcello,^{74a,74c} Z. X. Meng,⁶⁶ J. G. Messchendorp,^{13,64} G. Mezzadri,^{29a} H. Miao,^{1,63} T. J. Min,⁴²
 R. E. Mitchell,²⁷ X. H. Mo,^{1,58,63} B. Moses,²⁷ N. Yu. Muchnoi,^{4,c} J. Muskalla,³⁵ Y. Nefedov,³⁶ F. Nerling,^{18,e} L. S. Nie,²⁰
 I. B. Nikolaev,^{4,c} Z. Ning,^{1,58} S. Nisar,^{11,m} Q. L. Niu,^{38,k,l} W. D. Niu,⁵⁵ Y. Niu,⁵⁰ S. L. Olsen,⁶³ Q. Ouyang,^{1,58,63}
 S. Pacetti,^{28b,28c} X. Pan,⁵⁵ Y. Pan,⁵⁷ A. Pathak,³⁴ Y. P. Pei,^{71,58} M. Pelizaeus,³ H. P. Peng,^{71,58} Y. Y. Peng,^{38,k,l} K. Peters,^{13,e}
 J. L. Ping,⁴¹ R. G. Ping,^{1,63} S. Plura,³⁵ V. Prasad,³³ F. Z. Qi,¹ H. Qi,^{71,58} H. R. Qi,⁶¹ M. Qi,⁴² T. Y. Qi,^{12,g} S. Qian,^{1,58}
 W. B. Qian,⁶³ C. F. Qiao,⁶³ X. K. Qiao,⁸⁰ J. J. Qin,⁷² L. Q. Qin,¹⁴ L. Y. Qin,^{71,58} X. P. Qin,^{12,g} X. S. Qin,⁵⁰ Z. H. Qin,^{1,58}
 J. F. Qiu,¹ Z. H. Qu,⁷² C. F. Redmer,³⁵ K. J. Ren,³⁹ A. Rivetti,^{74c} M. Rolo,^{74c} G. Rong,^{1,63} Ch. Rosner,¹⁸ S. N. Ruan,⁴³
 N. Salone,⁴⁴ A. Sarantsev,^{36,d} Y. Schelhaas,³⁵ K. Schoenning,⁷⁵ M. Scodreggio,^{29a} K. Y. Shan,^{12,g} W. Shan,²⁴ X. Y. Shan,^{71,58}
 Z. J. Shang,^{38,k,l} J. F. Shangguan,¹⁶ L. G. Shao,^{1,63} M. Shao,^{71,58} C. P. Shen,^{12,g} H. F. Shen,^{1,8} W. H. Shen,⁶³ X. Y. Shen,^{1,63}
 B. A. Shi,⁶³ H. Shi,^{71,58} H. C. Shi,^{71,58} J. L. Shi,^{12,g} J. Y. Shi,¹ Q. Q. Shi,⁵⁵ S. Y. Shi,⁷² X. Shi,^{1,58} J. J. Song,¹⁹ T. Z. Song,⁵⁹
 W. M. Song,^{34,1} Y. J. Song,^{12,g} Y. X. Song,^{46,h,n} S. Sosio,^{74a,74c} S. Spataro,^{74a,74c} F. Stieler,³⁵ Y. J. Su,⁶³ G. B. Sun,⁷⁶
 G. X. Sun,¹ H. Sun,⁶³ H. K. Sun,¹ J. F. Sun,¹⁹ K. Sun,⁶¹ L. Sun,⁷⁶ S. S. Sun,^{1,63} T. Sun,^{51,f} W. Y. Sun,³⁴ Y. Sun,⁹ Y. J. Sun,^{71,58}
 Y. Z. Sun,¹ Z. Q. Sun,^{1,63} Z. T. Sun,⁵⁰ C. J. Tang,⁵⁴ G. Y. Tang,¹ J. Tang,⁵⁹ M. Tang,^{71,58} Y. A. Tang,⁷⁶ L. Y. Tao,⁷²
 Q. T. Tao,^{25,i} M. Tat,⁶⁹ J. X. Teng,^{71,58} V. Thoren,⁷⁵ W. H. Tian,⁵⁹ Y. Tian,^{31,63} Z. F. Tian,⁷⁶ I. Uman,^{62b} Y. Wan,⁵⁵
 S. J. Wang,⁵⁰ B. Wang,¹ B. L. Wang,⁶³ Bo Wang,^{71,58} D. Y. Wang,^{46,h} F. Wang,⁷² H. J. Wang,^{38,k,l} J. J. Wang,⁷⁶ J. P. Wang,⁵⁰
 K. Wang,^{1,58} L. L. Wang,¹ M. Wang,⁵⁰ N. Y. Wang,⁶³ S. Wang,^{12,g} S. Wang,^{38,k,l} T. Wang,^{12,g} T. J. Wang,⁴³ W. Wang,⁵⁹
 W. Wang,⁷² W. P. Wang,^{35,71,o} X. Wang,^{46,h} X. F. Wang,^{38,k,l} X. J. Wang,³⁹ X. L. Wang,^{12,g} X. N. Wang,¹ Y. Wang,⁶¹
 Y. D. Wang,⁴⁵ Y. F. Wang,^{1,58,63} Y. L. Wang,¹⁹ Y. N. Wang,⁴⁵ Y. Q. Wang,¹ Yaqian Wang,¹⁷ Yi Wang,⁶¹ Z. Wang,^{1,58}
 Z. L. Wang,⁷² Z. Y. Wang,^{1,63} Ziyi Wang,⁶³ D. H. Wei,¹⁴ F. Weidner,⁶⁸ S. P. Wen,¹ Y. R. Wen,³⁹ U. Wiedner,³ G. Wilkinson,⁶⁹
 M. Wolke,⁷⁵ L. Wollenberg,³ C. Wu,³⁹ J. F. Wu,^{1,8} L. H. Wu,¹ L. J. Wu,^{1,63} X. Wu,^{12,g} X. H. Wu,³⁴ Y. Wu,^{71,58} Y. H. Wu,⁵⁵
 Y. J. Wu,³¹ Z. Wu,^{1,58} L. Xia,^{71,58} X. M. Xian,³⁹ B. H. Xiang,^{1,63} T. Xiang,^{46,h} D. Xiao,^{38,k,l} G. Y. Xiao,⁴² S. Y. Xiao,¹
 Y. L. Xiao,^{12,g} Z. J. Xiao,⁴¹ C. Xie,⁴² X. H. Xie,^{46,h} Y. Xie,⁵⁰ Y. G. Xie,^{1,58} Y. H. Xie,⁶ Z. P. Xie,^{71,58} T. Y. Xing,^{1,63}
 C. F. Xu,^{1,63} C. J. Xu,⁵⁹ G. F. Xu,¹ H. Y. Xu,^{66,2,p} M. Xu,^{71,58} Q. J. Xu,¹⁶ Q. N. Xu,³⁰ W. Xu,¹ W. L. Xu,⁶⁶ X. P. Xu,⁵⁵
 Y. C. Xu,⁷⁷ Z. S. Xu,⁶³ F. Yan,^{12,g} L. Yan,^{12,g} W. B. Yan,^{71,58} W. C. Yan,⁸⁰ X. Q. Yan,¹ H. J. Yang,^{51,f} H. L. Yang,³⁴
 H. X. Yang,¹ T. Yang,¹ Y. Yang,^{12,g} Y. F. Yang,^{1,63} Y. F. Yang,⁴³ Y. X. Yang,^{1,63} Z. W. Yang,^{38,k,l} Z. P. Yao,⁵⁰ M. Ye,^{1,58}
 M. H. Ye,⁸ J. H. Yin,¹ Z. Y. You,⁵⁹ B. X. Yu,^{1,58,63} C. X. Yu,⁴³ G. Yu,^{1,63} J. S. Yu,^{25,i} T. Yu,⁷² X. D. Yu,^{46,h} Y. C. Yu,⁸⁰
 C. Z. Yuan,^{1,63} J. Yuan,³⁴ J. Yuan,⁴⁵ L. Yuan,² S. C. Yuan,^{1,63} Y. Yuan,^{1,63} Z. Y. Yuan,⁵⁹ C. X. Yue,³⁹ A. A. Zafar,⁷³
 F. R. Zeng,⁵⁰ S. H. Zeng,⁷² X. Zeng,^{12,g} Y. Zeng,^{25,i} Y. J. Zeng,⁵⁹ Y. J. Zeng,^{1,63} X. Y. Zhai,³⁴ Y. C. Zhai,⁵⁰ Y. H. Zhan,⁵⁹
 A. Q. Zhang,^{1,63} B. L. Zhang,^{1,63} B. X. Zhang,¹ D. H. Zhang,⁴³ G. Y. Zhang,¹⁹ H. Zhang,⁸⁰ H. Zhang,^{71,58} H. C. Zhang,^{1,58,63}
 H. H. Zhang,³⁴ H. H. Zhang,⁵⁹ H. Q. Zhang,^{1,58,63} H. R. Zhang,^{71,58} H. Y. Zhang,^{1,58} J. Zhang,⁸⁰ J. Zhang,⁵⁹ J. J. Zhang,⁵²
 J. L. Zhang,²⁰ J. Q. Zhang,⁴¹ J. S. Zhang,^{12,g} J. W. Zhang,^{1,58,63} J. X. Zhang,^{38,k,l} J. Y. Zhang,¹ J. Z. Zhang,^{1,63}
 Jianyu Zhang,⁶³ L. M. Zhang,⁶¹ Lei Zhang,⁴² P. Zhang,^{1,63} Q. Y. Zhang,³⁴ R. Y. Zhang,^{38,k,l} S. H. Zhang,^{1,63} Shulei Zhang,^{25,i}
 X. D. Zhang,⁴⁵ X. M. Zhang,¹ X. Y. Zhang,⁵⁰ Y. Zhang,⁷² Y. Zhang,¹ Y. T. Zhang,⁸⁰ Y. H. Zhang,^{1,58} Y. M. Zhang,³⁹
 Yan Zhang,^{71,58} Z. D. Zhang,¹ Z. H. Zhang,¹ Z. L. Zhang,³⁴ Z. Y. Zhang,⁷⁶ Z. Y. Zhang,⁴³ Z. Z. Zhang,⁴⁵ G. Zhao,¹

J. Y. Zhao,^{1,63} J. Z. Zhao,^{1,58} L. Zhao,¹ Lei Zhao,^{71,58} M. G. Zhao,⁴³ N. Zhao,⁷⁸ R. P. Zhao,⁶³ S. J. Zhao,⁸⁰ Y. B. Zhao,^{1,58}
 Y. X. Zhao,^{31,63} Z. G. Zhao,^{71,58} A. Zhemchugov,^{36,b} B. Zheng,⁷² B. M. Zheng,³⁴ J. P. Zheng,^{1,58} W. J. Zheng,^{1,63}
 Y. H. Zheng,⁶³ B. Zhong,⁴¹ X. Zhong,⁵⁹ H. Zhou,⁵⁰ J. Y. Zhou,³⁴ L. P. Zhou,^{1,63} S. Zhou,⁶ X. Zhou,⁷⁶ X. K. Zhou,⁶
 X. R. Zhou,^{71,58} X. Y. Zhou,³⁹ Y. Z. Zhou,^{12,g} J. Zhu,⁴³ K. Zhu,¹ K. J. Zhu,^{1,58,63} K. S. Zhu,^{12,g} L. Zhu,³⁴ L. X. Zhu,⁶³
 S. H. Zhu,⁷⁰ T. J. Zhu,^{12,g} W. D. Zhu,⁴¹ Y. C. Zhu,^{71,58} Z. A. Zhu,^{1,63} J. H. Zou,¹ and J. Zu^{71,58}

(BESIII Collaboration)

¹*Institute of High Energy Physics, Beijing 100049, People's Republic of China*

²*Beihang University, Beijing 100191, People's Republic of China*

³*Bochum Ruhr-University, D-44780 Bochum, Germany*

⁴*Budker Institute of Nuclear Physics SB RAS (BINP), Novosibirsk 630090, Russia*

⁵*Carnegie Mellon University, Pittsburgh, Pennsylvania 15213, USA*

⁶*Central China Normal University, Wuhan 430079, People's Republic of China*

⁷*Central South University, Changsha 410083, People's Republic of China*

⁸*China Center of Advanced Science and Technology, Beijing 100190, People's Republic of China*

⁹*China University of Geosciences, Wuhan 430074, People's Republic of China*

¹⁰*Chung-Ang University, Seoul, 06974, Republic of Korea*

¹¹*COMSATS University Islamabad, Lahore Campus, Defence Road, Off Raiwind Road, 54000 Lahore, Pakistan*

¹²*Fudan University, Shanghai 200433, People's Republic of China*

¹³*GSI Helmholtzcentre for Heavy Ion Research GmbH, D-64291 Darmstadt, Germany*

¹⁴*Guangxi Normal University, Guilin 541004, People's Republic of China*

¹⁵*Guangxi University, Nanning 530004, People's Republic of China*

¹⁶*Hangzhou Normal University, Hangzhou 310036, People's Republic of China*

¹⁷*Hebei University, Baoding 071002, People's Republic of China*

¹⁸*Helmholtz Institute Mainz, Staudinger Weg 18, D-55099 Mainz, Germany*

¹⁹*Henan Normal University, Xinxiang 453007, People's Republic of China*

²⁰*Henan University, Kaifeng 475004, People's Republic of China*

²¹*Henan University of Science and Technology, Luoyang 471003, People's Republic of China*

²²*Henan University of Technology, Zhengzhou 450001, People's Republic of China*

²³*Huangshan College, Huangshan 245000, People's Republic of China*

²⁴*Hunan Normal University, Changsha 410081, People's Republic of China*

²⁵*Hunan University, Changsha 410082, People's Republic of China*

²⁶*Indian Institute of Technology Madras, Chennai 600036, India*

²⁷*Indiana University, Bloomington, Indiana 47405, USA*

^{28a}*INFN Laboratori Nazionali di Frascati, I-00044 Frascati, Italy*

^{28b}*INFN Sezione di Perugia, I-06100, Perugia, Italy*

^{28c}*University of Perugia, I-06100, Perugia, Italy*

^{29a}*INFN Sezione di Ferrara, I-44122, Ferrara, Italy*

^{29b}*INFN Sezione di Ferrara, University of Ferrara, I-44122, Ferrara, Italy*

³⁰*Inner Mongolia University, Hohhot 010021, People's Republic of China*

³¹*Institute of Modern Physics, Lanzhou 730000, People's Republic of China*

³²*Institute of Physics and Technology, Peace Avenue 54B, Ulaanbaatar 13330, Mongolia*

³³*Instituto de Alta Investigación, Universidad de Tarapacá, Casilla 7D, Arica 1000000, Chile*

³⁴*Jilin University, Changchun 130012, People's Republic of China*

³⁵*Johannes Gutenberg University of Mainz, Johann-Joachim-Becher-Weg 45, D-55099 Mainz, Germany*

³⁶*Joint Institute for Nuclear Research, 141980 Dubna, Moscow region, Russia*

³⁷*Justus-Liebig-Universitaet Giessen, II. Physikalisches Institut, Heinrich-Buff-Ring 16, D-35392 Giessen, Germany*

³⁸*Lanzhou University, Lanzhou 730000, People's Republic of China*

³⁹*Liaoning Normal University, Dalian 116029, People's Republic of China*

⁴⁰*Liaoning University, Shenyang 110036, People's Republic of China*

⁴¹*Nanjing Normal University, Nanjing 210023, People's Republic of China*

⁴²*Nanjing University, Nanjing 210093, People's Republic of China*

⁴³*Nankai University, Tianjin 300071, People's Republic of China*

⁴⁴*National Centre for Nuclear Research, Warsaw 02-093, Poland*

⁴⁵*North China Electric Power University, Beijing 102206, People's Republic of China*

- ⁴⁶*Peking University, Beijing 100871, People's Republic of China*
⁴⁷*Qufu Normal University, Qufu 273165, People's Republic of China*
⁴⁸*Renmin University of China, Beijing 100872, People's Republic of China*
⁴⁹*Shandong Normal University, Jinan 250014, People's Republic of China*
⁵⁰*Shandong University, Jinan 250100, People's Republic of China*
⁵¹*Shanghai Jiao Tong University, Shanghai 200240, People's Republic of China*
⁵²*Shanxi Normal University, Linfen 041004, People's Republic of China*
⁵³*Shanxi University, Taiyuan 030006, People's Republic of China*
⁵⁴*Sichuan University, Chengdu 610064, People's Republic of China*
⁵⁵*Soochow University, Suzhou 215006, People's Republic of China*
⁵⁶*South China Normal University, Guangzhou 510006, People's Republic of China*
⁵⁷*Southeast University, Nanjing 211100, People's Republic of China*
⁵⁸*State Key Laboratory of Particle Detection and Electronics, Beijing 100049, Hefei 230026, People's Republic of China*
⁵⁹*Sun Yat-Sen University, Guangzhou 510275, People's Republic of China*
⁶⁰*Suranaree University of Technology, University Avenue 111, Nakhon Ratchasima 30000, Thailand*
⁶¹*Tsinghua University, Beijing 100084, People's Republic of China*
^{62a}*Turkish Accelerator Center Particle Factory Group, Istinye University, 34010, Istanbul, Turkey*
^{62b}*Near East University, Nicosia, North Cyprus, 99138, Mersin 10, Turkey*
⁶³*University of Chinese Academy of Sciences, Beijing 100049, People's Republic of China*
⁶⁴*University of Groningen, NL-9747 AA Groningen, The Netherlands*
⁶⁵*University of Hawaii, Honolulu, Hawaii 96822, USA*
⁶⁶*University of Jinan, Jinan 250022, People's Republic of China*
⁶⁷*University of Manchester, Oxford Road, Manchester M13 9PL, United Kingdom*
⁶⁸*University of Muenster, Wilhelm-Klemm-Strasse 9, 48149 Muenster, Germany*
⁶⁹*University of Oxford, Keble Road, Oxford OX13RH, United Kingdom*
⁷⁰*University of Science and Technology Liaoning, Anshan 114051, People's Republic of China*
⁷¹*University of Science and Technology of China, Hefei 230026, People's Republic of China*
⁷²*University of South China, Hengyang 421001, People's Republic of China*
⁷³*University of the Punjab, Lahore-54590, Pakistan*
^{74a}*University of Turin and INFN, University of Turin, I-10125, Turin, Italy*
^{74b}*University of Eastern Piedmont, I-15121, Alessandria, Italy*
^{74c}*INFN, I-10125, Turin, Italy*
⁷⁵*Uppsala University, Box 516, SE-75120 Uppsala, Sweden*
⁷⁶*Wuhan University, Wuhan 430072, People's Republic of China*
⁷⁷*Yantai University, Yantai 264005, People's Republic of China*
⁷⁸*Yunnan University, Kunming 650500, People's Republic of China*
⁷⁹*Zhejiang University, Hangzhou 310027, People's Republic of China*
⁸⁰*Zhengzhou University, Zhengzhou 450001, People's Republic of China*

^aDeceased.

^bAlso at the Moscow Institute of Physics and Technology, Moscow 141700, Russia.

^cAlso at the Novosibirsk State University, Novosibirsk 630090, Russia.

^dAlso at the NRC "Kurchatov Institute," PNPI, 188300 Gatchina, Russia.

^eAlso at Goethe University Frankfurt, 60323 Frankfurt am Main, Germany.

^fAlso at Key Laboratory for Particle Physics, Astrophysics and Cosmology, Ministry of Education; Shanghai Key Laboratory for Particle Physics and Cosmology; and Institute of Nuclear and Particle Physics, Shanghai 200240, People's Republic of China.

^gAlso at Key Laboratory of Nuclear Physics and Ion-beam Application (MOE) and Institute of Modern Physics, Fudan University, Shanghai 200443, People's Republic of China.

^hAlso at State Key Laboratory of Nuclear Physics and Technology, Peking University, Beijing 100871, People's Republic of China.

ⁱAlso at School of Physics and Electronics, Hunan University, Changsha 410082, China.

^jAlso at Guangdong Provincial Key Laboratory of Nuclear Science, Institute of Quantum Matter, South China Normal University, Guangzhou 510006, China.

^kAlso at MOE Frontiers Science Center for Rare Isotopes, Lanzhou University, Lanzhou 730000, People's Republic of China.

^lAlso at Lanzhou Center for Theoretical Physics, Lanzhou University, Lanzhou 730000, People's Republic of China.

^mAlso at the Department of Mathematical Sciences, IBA, Karachi 75270, Pakistan.

ⁿAlso at Ecole Polytechnique Federale de Lausanne (EPFL), CH-1015 Lausanne, Switzerland.

^oAlso at Helmholtz Institute Mainz, Staudinger Weg 18, D-55099 Mainz, Germany.

^pAlso at School of Physics, Beihang University, Beijing 100191, China.